Contents

Calibration of the MODIS Thermal Bands

Detailed Support Document to ATBD 1995

MCST Ref. No. G003

25 Oct 1995

Dan Knowles / GSC
Harry Montgomery / NASA
I. L. Goldberg / SWALES

MODIS Characterization Support Team
7501 Forbes Blvd. Suite 103

Section 1

MODIS Overview

MODIS uses HgCdTe detectors, operating at a temperature of 85 Kelvin, to sense radiation in the infrared portion of the radiometric spectrum. Each IR wavelength band has ten detectors in parallel (along track). The signal path from an individual detector to the output is called a channel. Each detector has a 1 kilometer Instantaneous Field Of View (IFOV) when imaging the Earth at nadir. Each band has a filter, also at 85 Kelvin, to permit a limited spectral range to irradiate its 10 constituent detectors. There are 16 infrared bands on the MODIS instrument with center wavelengths ranging from 3.75 µm to 14.235 µm (see Table 1). The short to midwave infrared bands (MODIS bands 20-25, 27-30) use photovoltaic detectors. The long wave infrared bands (MODIS bands 31-36) use photoconductive detectors.

MODIS uses two on-orbit calibrators (the OBC blackbody and space view) as reference targets from which it determines the spectral radiance emitted from the Earth and its atmosphere. A paddle wheel scan mirror is used to scan the optical line of sight of the detectors across the calibrators and the Earth's surface. The scan mirror is two sided, each side completing a scan with 180 degrees of mirror rotation. The duration of one scan (180 degree rotation of the scan mirror) is 1.4 seconds.

MODIS will be affixed to the EOS AM and EOS PM spacecraft (see Fig. 0). The AM series will have a sun-synchronous orbit with an equatorial descending crossing time of 10:30 AM. The PM series will have a sun-synchronous orbit with an equatorial ascending crossing time of 1:30 PM. The orbital altitude will be 705.3 km with a 98.21 degree inclination.

The velocity vector of the EOS AM spacecraft is defined as the positive x direction. The axis of the MODIS scan mirror is aligned with the x axis. The rotation of the scan mirror is in the positive x direction as defined by the right hand rule. The view point of Figures 1 - 3, which is a cutout view of the key infrared components in the MODIS scan cavity, is such that the scan mirror rotates in the clockwise direction. The vector extending from the scan mirror axis to approximately the center of the Earth view porthole defines the positive z direction. During normal spacecraft operations, the positive z direction will be aligned with Earth nadir.

Band	Center Wavelength
20	3.750µm
21	3.959µm
22	3.959µm
23	4.050µm
24	4.465µm
25	4.515µm
27	6.715µm
28	7.325µm
29	8.550µm
30	9.730µm
31	11.030µm
32	12.020µm
33	13.335µm
34	13.635µm
35	13.935µm
36	14.235µm

Table 1. MODIS center wavelengths

As the scan mirror rotates in the positive x direction, an angle is traced out between the optical line of sight and the positive z axis. This angle is referred to as the MODIS scan (or view) angle. This angle extends across 360 degrees of geometric space for 180 degrees of mirror rotation. The optical axis is located at an angle of 284 degrees with respect to the positive z axis.

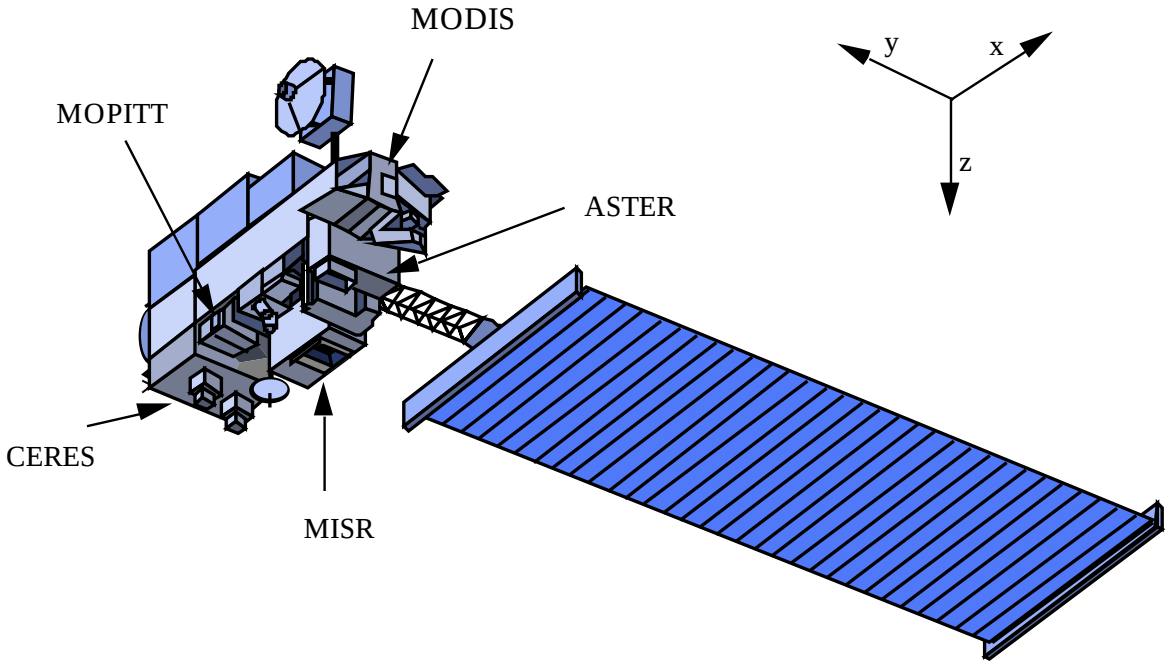

Figure 0. EOS AM & EOS PM Spacecraft

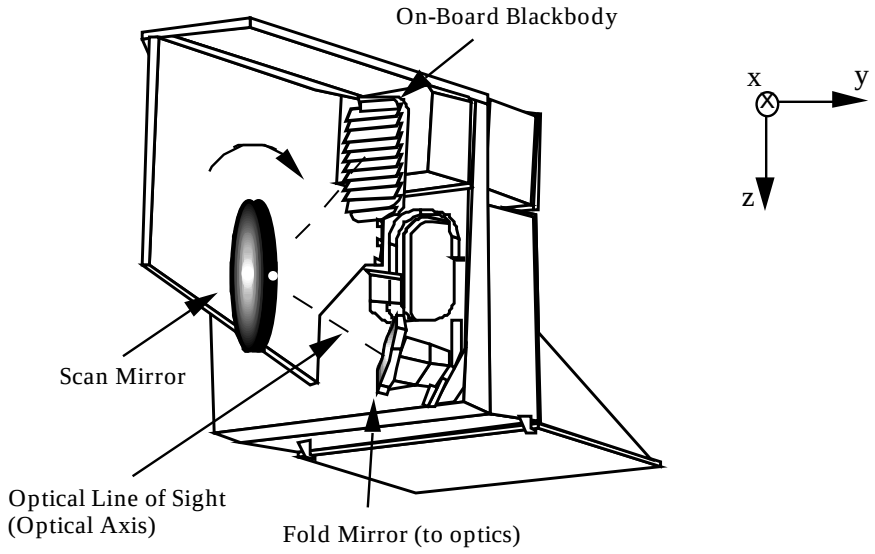

Figure 1. MODIS scan of the on-board blackbody

The first calibrator of concern to infrared calibration is the OBC blackbody. This is a v-groove structure constructed of anodized aluminum with 12 embedded thermistors. According to the MODIS specification for the on-board blackbody, the emissivity will be no less than .992, known to .004 with an effective blackbody temperature known to .1 Kelvin. The on-board blackbody is the "hot" calibration target with a nominal ambient operating temperature of 285 Kelvin, and an optional heated mode temperature of 315 Kelvin. The scan mirror has a nominal view angle 231.4 degrees while imaging the blackbody with a nominal angle of incidence between the optical axis and the scan mirror normal of 26.30 degrees. MODIS collects 15 data points (pixels) during each scan of the blackbody covering an angular span of 16 IFOV. Figure 1 illustrates the scan mirror positioning and optical line of sight while MODIS is imaging the on-board blackbody.

The second calibrator of concern to infrared calibration is the space view. This is a porthole in the MODIS cavity which has a direct view of space. Space is the "cold" calibration target with an effective temperature on the order of 3 Kelvin. The scan mirror has a nominal view angle of 261.2 degrees while imaging the space view with a nominal angle of incidence between the optical axis and the scan mirror normal of 11.42 degrees. MODIS collects 15 data points (pixels) during each scan of the space view covering an angular span of 16 IFOV. Figure 2 illustrates the scan mirror positioning and optical line of sight while MODIS is imaging space through the space view porthole.

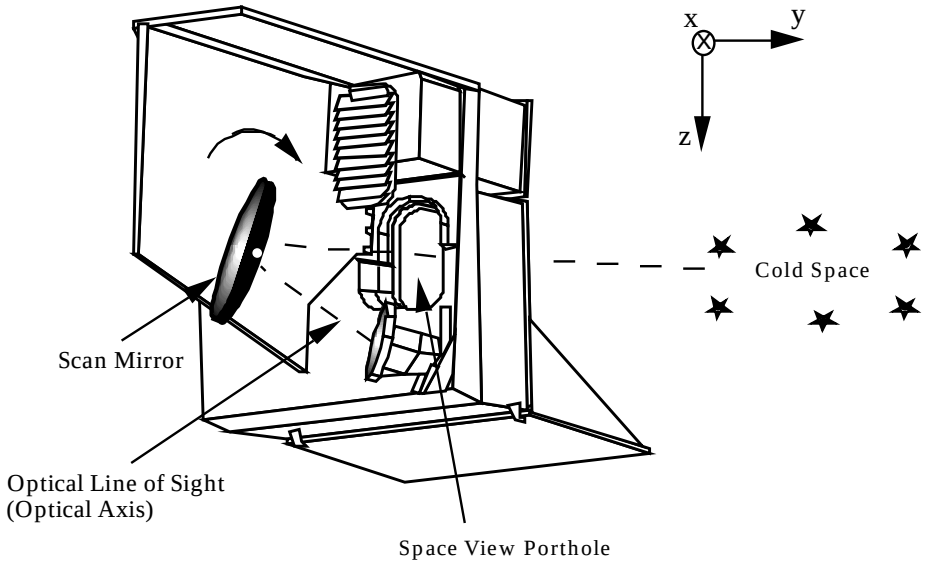

Figure 2. MODIS scan of the space view

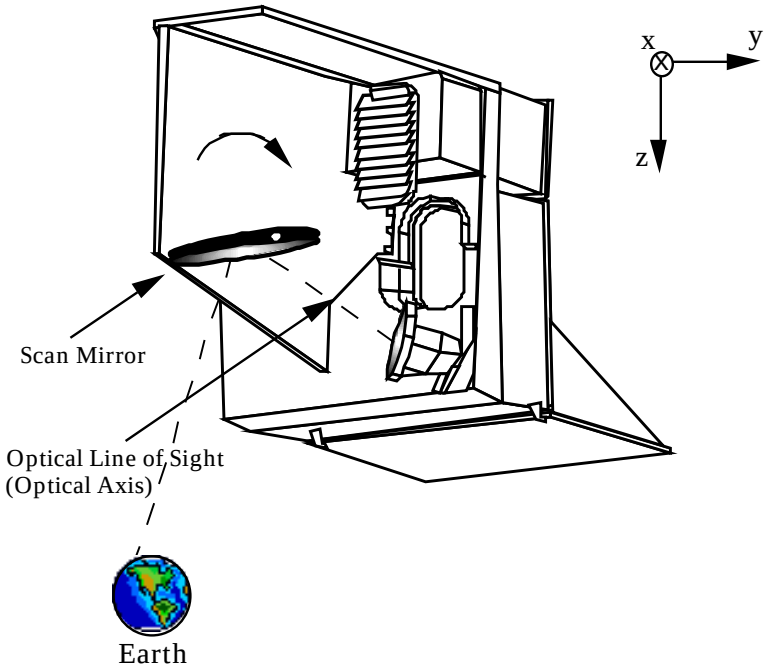

Figure 3. MODIS scan of the Earth

The third important infrared region in the MODIS scan is the scan of the Earth through the Earth view porthole. The scan mirror begins the scan of Earth with a nominal view angle of -55 degrees and a nominal angle of incidence between the optical axis and the scan

mirror normal of 10.5 degrees. The scan mirror ends the scan of Earth with a nominal view angle of 55 degrees and a nominal angle of incidence between the optical axis and the scan mirror normal of 65.5 degrees. 1354 data points (pixels) are collected corresponding to an angular span of 1355 IFOV. Figure 3 illustrates the scan mirror positioning and optical line of sight while MODIS is imaging an Earth scene through the Earth view porthole.

The scan mirror has a reflectivity which significantly varies with scan angle. This is primarily due to the SiOx coating on the mirror. Due to this phenomena, a rather complex calibration algorithm is needed to correct for this angular reflectivity variation of the scan mirror. This necessitates a full roll of the spacecraft during orbit in order to view space through the entire Earth view porthole. The pixel variations across this view of a "uniform" target will provide the means to correct for errors in the pre-launch measurement of the scan mirror relative reflectivity as well as correct for the effects of contamination across the mirror's surface. The contamination for larger Earth view angles is expected to be greater than for the smaller angles. This is because the larger angle has a focal plane "footprint" which extends closer to the edges of the scan mirror, which span more space than the center regions.

Section 2

Thermal Band Calibration

Summary

The MODIS Level 1B calibration algorithm for the thermal bands is designed to determine the apparent spectral radiance (with associated uncertainties) for each pixel observed through the Earth view. The Level 1B radiance product (see Section 4) is

$$L_{ev} = \frac{\sum_{\lambda=\lambda_1}^{\lambda_n} L_{\lambda,ev} R_{\lambda,tot} \Delta\lambda}{\sum_{\lambda=\lambda_1}^{\lambda_n} R_{\lambda,tot} \Delta\lambda}$$

To track on-orbit changes in the instrument, the thermal bands will be recalibrated every scan. Improvements over the 1994 ATBD involve detector nonlinearity, scan mirror reflectivity variations with scan angle, optical background corrections and pre-launch testing requirements. Some issues under current consideration with details pending are polarization and spurious effects.

Calibration Coefficients

Through careful mathematical manipulation of the terms of the detector power equation presented in this document (see Section 3), all necessary parameters can be sufficiently determined on-orbit with just two calibrators. These parameters are determined as a group and not individually and the groups are referred to as "calibration coefficients".

A MODIS infrared calibration coefficient is a deliberate mathematical grouping of the individual parameters of the pre-amplified focal plane voltage relationship to the detector power, considered invariant for a period of one scan line, not directly measured, but determined from the telemetry pertaining to relevant reference radiance sources. These coefficients will be adjusted every scan on-orbit to correct for changes since the pre-launch measurements.

Top-Level Algorithm

The Level 1B calibrated Earth scene apparent spectral radiance can be determined by Eq. 31. Two of the calibration coefficients (m & L_o)are obtained every scan from OBC blackbody

and space view data (see Section 4). The nonlinear term, α, will be determined from the thermal vacuum tests for several sets of instrument conditions and treated as a constant unique to each combination of instrument and detector temperatures for the life of the mission (see Section 6). Fig. 4 portrays the temperature conditions for the current protoflight test plan (check marks denote planned tests).

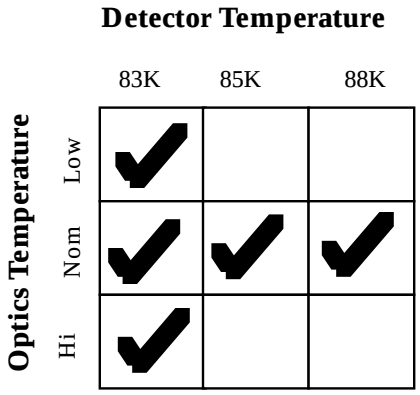

Fig 4. Current Protoflight Test Plan

Space View

The space view is the cold (zero scene radiance) calibration source. However, there will be some nonspecular radiance from the scan mirror while scanning the space view and a correction term for scan cavity edge contributions is included. If the BRDF of the scan mirror is well understood, this correction term could be adjusted based on the cavity temperature local to the space view. The current approach will set this term equal to zero.

15 space view pixels will be available each scan for calibration. Because up to 30 space view pixels are used to determine an effective space view signal, many of these measurements will fall below the average. This is natural because of the effects of noise. This brings about the issue of possible negative radiance calibration products for cold Earth scenes. This is permissible as long it falls within the uncertainty bars. Exceptions will be appropriately flagged.

OBC Blackbody

The OBC blackbody is the warm calibration source. The radiance of the OBC blackbody incident upon the scan mirror can be determined every scan with the data from the twelve embedded blackbody thermistors (see Section 7).

Traceability to NIST of the OBC blackbody temperature will be done directly through the OBC blackbody thermistors. Traceability of the OBC blackbody emissivity will be done through the thermistors of the BCS (see Section 9).

Outlier Rejection: OBC Blackbody Temperature

For each scan we will determine the three hottest and three coldest values of the twelve OBC blackbody thermistors (naming these six thermistors "mavericks" and the remaining six thermistors as "central"). The central thermistor values will be averaged to obtained a reference blackbody temperature with which to compare the "maverick" thermistors. The "maverick" thermistors which deviate from the reference blackbody temperature by greater than .052K (the acceptable gradient) will be considered "rejected" for that scan and appropriately flagged. The remaining thermistors will be averaged to obtain an effective blackbody temperature for the scan.

Outlier Rejection: OBC Blackbody and Space View Counts

For each scan we will determine the three highest and three lowest values of the fifteen OBC blackbody DN values (naming these six DN value "mavericks" and the remaining nine DN values "central"). The central DN values will be averaged to obtained a reference DN value with which to compare the "maverick" DN values. The "maverick" DN values which deviate from this reference DN value by an amount greater than the acceptable noise range (determined off-line) will be rejected for that scan and appropriately flagged. The remaining DN values will be averaged to obtain an average OBC blackbody DN value for the scan.

The same process described above for the OBC blackbody DN values will be performed on the space view DN values.

Scan Mirror Reflectivity

The reflectivity of the scan mirror for each detector, mirror side, and scan angle is needed for the thermal calibration algorithm. Some of this may be measured by SBRC for the actual MODIS scan mirror, or data will be obtained from witness sample testing. The most important measurements pertain to the pre-launch and on-orbit calibrator angles of incidence. The other angular values may be inferred by curve fitting these data.

A spacecraft maneuver is currently planned whereby the entire Earth view port can achieve a clear view of space. This provides a hot radiant source (OBC blackbody) and a cold source (space) viewed through the Earth view porthole at the pixels corresponding to the OBC blackbody angle of incidence. Therefore, scan angle independent calibration coefficients can be obtained and used to determine the scan mirror reflectance correction factor, D_s, for the space view and the remaining Earth view pixels. This correction factor is relative to a value at the blackbody angle of incidence and will be averaged over many scans to reduce the effects of $1/f$ noise.

Absolute reflectivity calibration is obtained because the calibration coefficients calibrate out the absolute reflectivity of the scan mirror at the blackbody view angle, and the scan angle

coefficients periodically adjusted to calibrate out the relative reflectivity contribution (see Section 5).

Noise Reduction

The OBC blackbody and space view signals will both be linearly interpolated across each scan line to reduce 1/f noise. This interpolation will be done using the same side of the scan mirror to avoid reflectance complications.

Data Requirements

The Level 1A data requirements for the Level 1B thermal calibration are the current scan (i) and scan (i+2) occurring two scans later. This allows independent processing for each side of the 2-sided scan mirror. Therefore, if data fails for scan (i+2), then scan (i) cannot be calibrated according to the standard baseline approach. For this event, a single scan calibration approach will be used with an appropriate flag.

Electronic Calibration and DC Restore

In order to subtract off optical background and bias power, MODIS uses an offset voltage based on the digital output while viewing space. This enables the A/D converter to stay on scale. This aspect of DC restore is executed every scan line based upon data from the previous scan line. Electronic gains are applied to the focal plane voltages based upon the digital output difference between the OBC blackbody and space view. This enables the dynamic range of the 12 bit A/D converter to be used to its potential. These applied gains will not be changed every scan, but may be changed periodically as needed. Because of these on-orbit electronic adjustments, it is necessary to convert the digital counts, gains, and offsets into the focal plane voltage. This will enable pre-launch measurements to be incorporated in the on-orbit calibration algorithm (see Section 8).

Spectral Calibration

The primary optical element in the spectral shape of the optical transmission is the band pass filter. Ideally the spectral shape of the whole system should be measured for each detector's optical path.

Adverse Calibration Events

A Lunar viewing through the space view will render the space view temporarily useless as a zero based calibration source. By monitoring the offset voltage and digital counts of the space view independent of ephemeris data, it is possible to determine when the moon is affecting the space view signal. These scans can be calibrated by freezing the calibration coefficients from the scan just before the lunar effect occurs. This calibration must be appropriately flagged.

By tracking both the OBC blackbody and the space view voltages, it is possible to determine whether the reflected OBC blackbody radiance increases as the solar diffuser is illuminated. If possible, an algorithm will be developed to account for this increase in reflected OBC blackbody radiance. SRCA operations can also affect thermal calibration. This will most likely be less significant than the solar diffuser illumination, however, the technique for correcting for this will be similar.

Lunar Calibration Product

Similar to the Level 1B Earth scene spectral radiance product, a Level 1B Lunar scene spectral radiance product will be determined from the space view signal during a lunar viewing through the space view.

Spurious Effects

Spurious effects can occur one of two possible ways: 1) while viewing the calibration source, in which case, the calibration coefficients are affected, 2) while viewing the Earth scene scan, in which case, the effects are implemented after the calibrated Earth scene spectral radiance is determined.

Ghosting effects, optical scattering effects, and within-band optical crosstalk should have little effect on the calibration coefficients. While scanning the OBC blackbody, which has a minimal thermal gradient, the image of the OBC fills the entire focal plane, with each detector viewing about 60% of the area of the blackbody. While scanning space, each detector images 1.4 mrad of space, and unless some substantial cosmic phenomena is present, this region can be considered uniform. Out of band crosstalk when viewing the blackbody will need to be analyzed

Spurious effects which occur during the Earth view scan are substantial. Of these effects, scattering appears to be the most significant. A model which simulates the effects of ghosting and scattering has been developed and a model for crosstalk effects is planned.

Vicarious Calibration

In order to use a vicarious source, its credibility must be demonstrated prior to its use with MODIS. Vicarious measurements could be utilized to correct for on-orbit OBC emissivity and detector nonlinearity changes.

Radiometric Uncertainties

A model of the MODIS instrument was produced to generate MODIS output using realistic nominal parameters. The calibration algorithm was then applied to this data with expected errors perturbed one at a time for each of the calibration parameters. A root-sum-square of these individual errors then gave a means for an analysis of the thermal calibration error.

Table 1 shows these results for all the MODIS bands, listing also the MODIS specification values. These results are by no means definitive because uncertainties of many individual parameters have not been clearly established yet. Included within this analysis are the effects of the uncertainty in: OBC blackbody temperature, OBC blackbody emissivity, scan cavity temperature, scan mirror temperature, nonlinearity, digitization, 1/f noise, center wavelength, scan mirror relative reflectivity, DC restore, and ghosting. Scattering and crosstalk are not currently included within these results.

MODIS Band	Radiometric Error	MODIS Spec
20	1.07%	0.8%
21	7.09%	10.0%
22	1.02%	1.0%
23	0.99%	1.0%
24	1.09%	1.0%
25	0.95%	1.0%
27	0.74%	1.0%
28	0.56%	1.0%
29	0.28%	1.0%
30	0.49%	1.0%
31	0.23%	0.5%
32	0.23%	0.5%
33	0.42%	1.0%
34	0.45%	1.0%
35	0.49%	1.0%
36	0.66%	1.0%
31hi	3.45%	10.0%
32hi	2.80%	10.0%

Table 1. Current Predicted Radiometric Uncertainties in percent of Ltyp

Part of the Level 1B product will be the uncertainties for each calibrated Earth scene pixel. This will be achieved with on-orbit data, perturbing each of the algorithm parameters by a specified amount whereby an Earth scene radiance error can be compared with the unperturbed Level 1B Earth scene radiance product. A root sum square of all these perturbations will yield an uncertainty unique to every Earth scene pixel.

Section 3

Mathematical Derivation

Infrared detection must be addressed from the point of view of the detector since a majority of the detector incident radiant flux originates from within the optical system.

The Quadratic Fit

This algorithm is essentially a hybrid of the SBRC approach and the historically accepted approaches, with the key difference being the accountability of optical background changes and detector nonlinearity on-orbit. This accountability is made possible through both the DC restore offset voltage, which has not previously been in the telemetry of other satellites, and the temperature measurements of the optics and detector. This additional telemetry will make it possible to transform the electronic output counts of the instrument into the focal plane voltage, V_s. In its basic form, the algorithm is based on the relationship between V_s and the total power applied to the detector which includes both the detector incident radiant flux and Joule heating (Fig. 5 and Eq. 1).

$$V_s = a\left(\Phi_s + P_x\right)^2 + b\left(\Phi_s + P_x\right) \tag{1}$$

where

Φ_s detector incident radiant flux attributed solely to the scan mirror and scene

P_x detector background flux and bias power (Joule heating).

a second order detector gain terms.

b first order detector gain terms.

This relationship is assumed quadratic for the somewhat limited range of detector incident radiant power. All calibration and scene reference points occur within this range and the term Px is determined by extrapolating to the zero detector voltage condition.

Because MODIS applies differing offset voltages every scan, and may periodically alter the electronic gains, a two point nonlinear calibration approach cannot be done solely on the basis of counts. MODIS counts have no meaning without their respective applied gains and offset voltage values. Therefore, the calibration curve will be expressed in terms of the pre-amplified voltage across the load resistor for the photoconductive bands and the pre-amplified voltage across the detector for the photovoltaic bands. This differentiation is useful since we desire these pre-amplified voltages to increase with an increase in detector flux for both the PC and PV bands, enabling the equation to apply equally to both types.

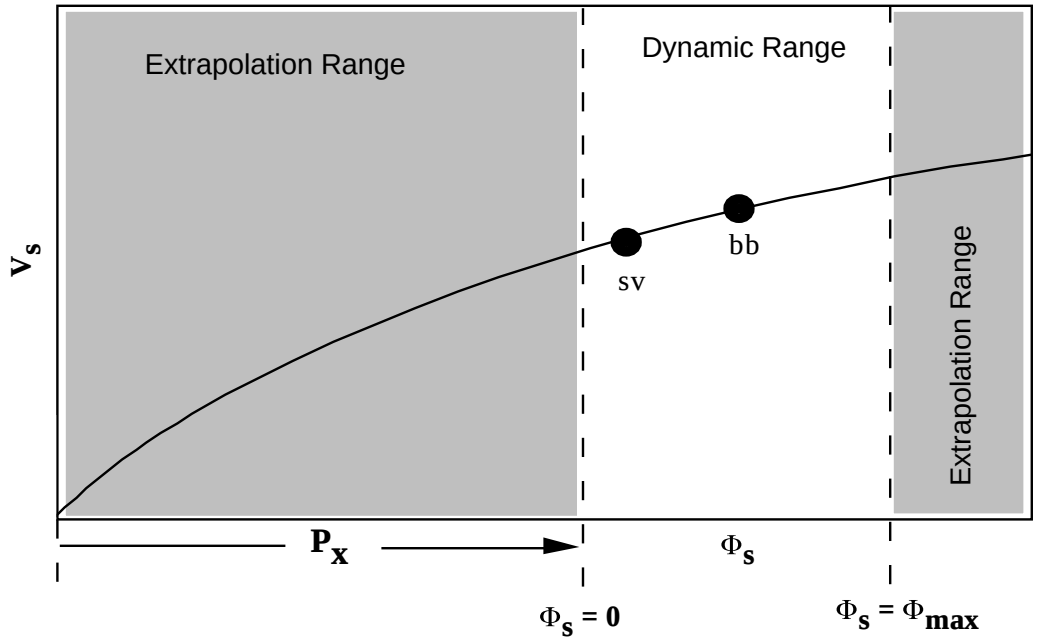

Fig. 5. Thermal band calibration curve. For any single scan, P_X is assumed invariant. P_X varies with instrument temperature, thereby removing much of the variance with instrument temperature from the nonlinear term.

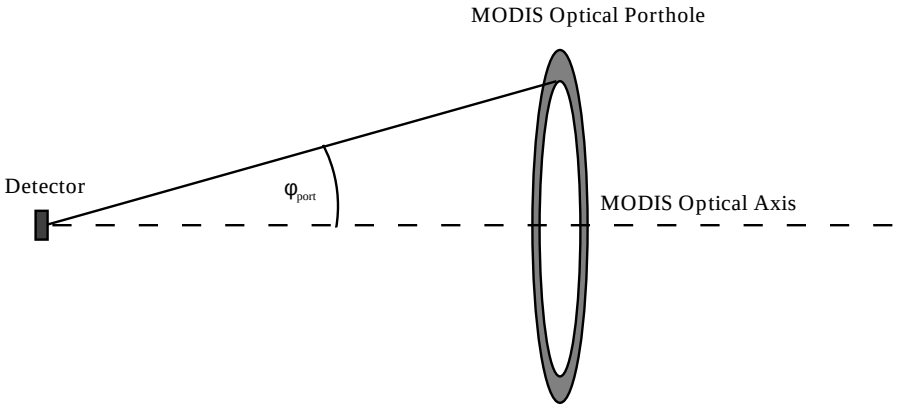

Figure 6. Effective Optical Acceptance Angle

For a full aperture optical system of transmission $\tau_{\lambda,opt}$, the detector incident radiant flux due solely to an external Lambertian source $L_{\lambda,s}$ can be expressed as

$$\Phi_s = \frac{\pi A_d}{4\left(f_{eff}^{\#}\right)^2} \int_{\lambda=0}^{\infty} L_{\lambda,s}\tau_{\lambda,opt}d\lambda \qquad (2)$$

where A_d is the image area of the detector and $f^{\#}_{eff}$ is the effective focal ratio, which for a symmetrical optical system and an unimmersed detector is defined as:

$$f^{\#}_{eff} = \frac{1}{2\sin\varphi_{port}} \tag{3}$$

where φ_{port} is the acceptance angle (see Fig. 6).

Detector Flux Due To The Scan Mirror and Scene

Because MODIS has a revolving SiOx coated scan mirror in front of the optics the transmission of the optical system will vary with scan angle. This will result in significantly differing scan mirror reflectance properties for each of the calibrators and the Earth scene. It is therefore useful to consider two classes of optics: static and dynamic. Static optics are those lenses, mirrors, and filters from the first fold mirror to the detector which do not vary their transmission properties between calibrators by changing their angular orientation. Dynamic optics refers to the scan mirror which views the blackbody, cold space, and the Earth at differing angles of incidence. This calibration approach treats these two classes of optics separately.

Since it is not practical to express real transmission data in functional form, the detector flux equation is best expressed in summation form. Treating the radiance exiting the MODIS scan mirror (which has a reflectivity of $\rho_{\lambda,s}$) as a Lambertian source, Eq. 2 becomes

$$\Phi_s = \frac{\pi A_d}{4\left(f^{\#}_{eff}\right)^2} \sum_{\lambda=\lambda_1}^{\lambda_n} \left(\left(1-\rho_{\lambda,s}\right)B_{\lambda,mir} + \rho_{\lambda,s}L_{\lambda,s}\right)\tau_{\lambda,s}\Delta\lambda \tag{4}$$

where $B_{\lambda,mir}$ is the Planck function applied to the temperature of the scan mirror and $L_{\lambda,s}$ is the spectral radiance incident upon the scan mirror from any arbitrary source.

In order to express Eq. 4 on-orbit to account for changes since pre-launch testing, the superscript "on-orbit" will be used to denote the actual on-orbit value, whereas the same term without the superscript will refer to the pre-launch measured value. Rearranging this equation to group the scan mirror reflectivity terms yields

$$\Phi_s = \frac{\pi A_d}{4\left(f^{\#}_{eff}\right)^2} \sum_{\lambda=\lambda_1}^{\lambda_n} \left(B_{\lambda,mir} + \rho^{on-orbit}_{\lambda,s}\left(L_{\lambda,s} - B_{\lambda,mir}\right)\right)\tau^{on-orbit}_{\lambda,s}\Delta\lambda \tag{5}$$

The optical properties will change over time due to contamination and temperature variations of the optics. In order to correct for these changes on-orbit, it is necessary to consider them spectrally uniform across each band. Furthermore, the ground values for optical transmission will most likely contain a certain amount of error. This measurement error is analogous to on-orbit transmission changes and is treated as such. Since the accountability for these on-orbit changes and ground measurement errors must be treated as a spectrally uniform change across the band, it is advisable to get a reasonable measurement of the optical transmission properties pre-launch.

We define a correction term for the on-orbit static optics transmission as

$$k_{\lambda,opt} = \frac{\tau_{\lambda,opt}^{on-orbit}}{\tau_{\lambda,opt}} \tag{6}$$

The pre-launch transmission of the static optics can be expressed as

$$\tau_{\lambda,opt} = T_{opt} R_{\lambda,opt} \tag{7}$$

where the integrated transmittance is defined as

$$T_{opt} = \sum_{\lambda=\lambda_1}^{\lambda_n} \tau_{\lambda,opt} \Delta\lambda$$

and the normalized spectral transmittance is defined as

$$R_{\lambda,opt} = \frac{\tau_{\lambda,opt}}{T_{opt}}$$

Combining Eqs. 6 & 7, the on-orbit transmission can be expressed in terms of the pre-launch normalized measurements and the on-orbit static optics correction term

$$\tau_{\lambda,opt}^{on-orbit} = k_{\lambda,opt} T_{opt} R_{\lambda,opt} \tag{10}$$

Applying Eq. 10 to Eq. 5, the detector flux due to the scene and the scan mirror can be expressed as

$$\Phi_s = \frac{\pi A_d}{4\left(f_{eff}^{\#}\right)^2} \sum_{\lambda=\lambda_1}^{\lambda_n} \left(B_{\lambda,mir} + \rho_{\lambda,s}^{on-orbit} \left(L_{\lambda,s} - B_{\lambda,mir} \right) \right) k_{\lambda,opt} T_{opt} R_{\lambda,opt} \Delta\lambda \tag{11}$$

Treating the static optics correction term as spectrally uniform across the band, an average value may be factored out of the summation. We may also factor out the total integrated pre-launch optical transmission, since it is not wavelength dependent. Therefore,

$$\Phi_s = \frac{\pi A_d T_{opt} k_{opt}}{4\left(f_{eff}^{\#}\right)^2} \sum_{\lambda=\lambda_1}^{\lambda_n} \left(B_{\lambda,mir} + \rho_{\lambda,s}^{on-orbit}\left(L_{\lambda,s} - B_{\lambda,mir}\right)\right) R_{\lambda,opt}\Delta\lambda \tag{12}$$

We define a correction term for the on-orbit reflectivity of the dynamic optics (scan mirror) as

$$\delta_{\lambda,s} = \frac{\rho_{\lambda,s}^{on-orbit}}{\rho_{\lambda,s}} \tag{14}$$

Applying this to Eq. 12 yields

$$\Phi_s = \frac{\pi A_d T_{opt} k_{opt}}{4\left(f_{eff}^{\#}\right)^2} \sum_{\lambda=\lambda_1}^{\lambda_n} B_{\lambda,mir} R_{\lambda,opt}\Delta\lambda + \frac{\pi A_d T_{opt} k_{opt}}{4\left(f_{eff}^{\#}\right)^2} \sum_{\lambda=\lambda_1}^{\lambda_n} \delta_{\lambda,s}\rho_{\lambda,s}\left(L_{\lambda,s} - B_{\lambda,mir}\right) R_{\lambda,opt}\Delta\lambda \tag{15}$$

Treating the scan mirror correction term as spectrally uniform across the band, an average value may be factored out of the summation in Eq. 15.

$$\Phi_s = \frac{\pi A_d T_{opt} k_{opt}}{4\left(f_{eff}^{\#}\right)^2} \sum_{\lambda=\lambda_1}^{\lambda_n} B_{\lambda,mir} R_{\lambda,opt}\Delta\lambda + \frac{\pi A_d T_{opt} k_{opt}\delta_s}{4\left(f_{eff}^{\#}\right)^2} \sum_{\lambda=\lambda_1}^{\lambda_n} \rho_{\lambda,s}\left(L_{\lambda,s} - B_{\lambda,mir}\right) R_{\lambda,opt}\Delta\lambda \tag{16}$$

The Detector Power Equation

Applying Eq. 16 to the pre-amplified voltage relationship (Eq. 1) yields

$$V_s = a\left(P_x + \frac{\pi A_d T_{opt} k_{opt}}{4\left(f_{eff}^{\#}\right)^2} \sum_{\lambda=\lambda_1}^{\lambda_n} B_{\lambda,mir} R_{\lambda,opt}\Delta\lambda + \frac{\pi A_d T_{opt} k_{opt}\delta_s}{4\left(f_{eff}^{\#}\right)^2} \sum_{\lambda=\lambda_1}^{\lambda_n} \rho_{\lambda,s}\left(L_{\lambda,s} - B_{\lambda,mir}\right) R_{\lambda,opt}\Delta\lambda\right)^2 + b\left(P_x + \frac{\pi A_d T_{opt} k_{opt}}{4\left(f_{eff}^{\#}\right)^2} \sum_{\lambda=\lambda_1}^{\lambda_n} B_{\lambda,mir} R_{\lambda,opt}\Delta\lambda + \frac{\pi A_d T_{opt} k_{opt}\delta_s}{4\left(f_{eff}^{\#}\right)^2} \sum_{\lambda=\lambda_1}^{\lambda_n} \rho_{\lambda,s}\left(L_{\lambda,s} - B_{\lambda,mir}\right) R_{\lambda,opt}\Delta\lambda\right) \tag{18}$$

We may selectively group terms which can be considered invariant across a single scan and therefore can be treated as calibration coefficients.

$$V_s = a\left(\frac{\pi A_d T_{opt} k_{opt}}{4\left(f_{eff}^{\#}\right)^2} \div \left(\frac{4P_x\left(f_{eff}^{\#}\right)^2}{\pi A_d T_{opt} k_{opt}} + \sum_{\lambda=\lambda_1}^{\lambda_n} B_{\lambda,mir} R_{\lambda,opt} \Delta\lambda + \delta_s \sum_{\lambda=\lambda_1}^{\lambda_n} \rho_{\lambda,s}\left(L_{\lambda,s} - B_{\lambda,mir}\right) R_{\lambda,opt} \Delta\lambda\right)^2\right)$$
$$+ b\left(\frac{\pi A_d T_{opt} k_{opt}}{4\left(f_{eff}^{\#}\right)^2} \div \left(\frac{4P_x\left(f_{eff}^{\#}\right)^2}{\pi A_d T_{opt} k_{opt}} + \sum_{\lambda=\lambda_1}^{\lambda_n} B_{\lambda,mir} R_{\lambda,opt} \Delta\lambda + \delta_s \sum_{\lambda=\lambda_1}^{\lambda_n} \rho_{\lambda,s}\left(L_{\lambda,s} - B_{\lambda,mir}\right) R_{\lambda,opt} \Delta\lambda\right)\right) \quad (19)$$

To create calibration coefficients which are relative to the scan mirror reflectivity at the OBC blackbody scan angle, multiply the numerator and denominator of Eq. 19 by δ_{bb}.

$$V_s = a\left(\frac{\pi A_d T_{opt} k_{opt} \delta_{bb}}{4\left(f_{eff}^{\#}\right)^2} \div \left(\frac{4P_x\left(f_{eff}^{\#}\right)^2}{\pi A_d T_{opt} k_{opt} \delta_{bb}} + \frac{1}{\delta_{bb}} \sum_{\lambda=\lambda_1}^{\lambda_n} B_{\lambda,mir} R_{\lambda,opt} \Delta\lambda + \frac{\delta_s}{\delta_{bb}} \sum_{\lambda=\lambda_1}^{\lambda_n} \rho_{\lambda,s}\left(L_{\lambda,s} - B_{\lambda,mir}\right) R_{\lambda,opt} \Delta\lambda\right)^2\right)$$
$$+ b\left(\frac{\pi A_d T_{opt} k_{opt} \delta_{bb}}{4\left(f_{eff}^{\#}\right)^2} \div \left(\frac{4P_x\left(f_{eff}^{\#}\right)^2}{\pi A_d T_{opt} k_{opt} \delta_{bb}} + \frac{1}{\delta_{bb}} \sum_{\lambda=\lambda_1}^{\lambda_n} B_{\lambda,mir} R_{\lambda,opt} \Delta\lambda + \frac{\delta_s}{\delta_{bb}} \sum_{\lambda=\lambda_1}^{\lambda_n} \rho_{\lambda,s}\left(L_{\lambda,s} - B_{\lambda,mir}\right) R_{\lambda,opt} \Delta\lambda\right)\right) \quad (20)$$

Equation 20 is now arranged such that it can be reduced to three calibration coefficients (m, q, L_o) which are considered invariant across one scan line. These calibration coefficients are

$$L_o = \frac{4P_x\left(f_{eff}^{\#}\right)^2}{\pi A_d T_{opt} k_{opt} \delta_{bb}} + \frac{1}{\delta_{bb}} \sum_{\lambda=\lambda_1}^{\lambda_n} B_{\lambda,mir} R_{\lambda,opt} \Delta\lambda \quad (21)$$

$$m = \frac{b\pi A_d T_{opt} k_{opt} \delta_{bb}}{4\left(f_{eff}^{\#}\right)^2} \quad (22)$$

$$q = a\left(\frac{\pi A_d T_{opt} k_{opt} \delta_{bb}}{4\left(f_{eff}^{\#}\right)^2} \div\right)^2 \quad (23)$$

Expressed in terms of these three calibration coefficients, the detector power equation (Eq. 20) becomes

$$V_s = q\left(L_o + D_s \sum_{\lambda=\lambda_1}^{\lambda_n} \rho_{\lambda,s}\left(L_{\lambda,s} - B_{\lambda,mir}\right) R_{\lambda,opt} \Delta\lambda \div\right)^2 + m\left(L_o + D_s \sum_{\lambda=\lambda_1}^{\lambda_n} \rho_{\lambda,s}\left(L_{\lambda,s} - B_{\lambda,mir}\right) R_{\lambda,opt} \Delta\lambda \div\right) \quad (24)$$

where the correction term for the on-orbit change in the reflectivity of the scan mirror relative to the value at the OBC blackbody view angle is

$$D_s = \frac{\delta_s}{\delta_{bb}} \tag{24a}$$

From Eq. 22 and Eq. 23 it can be noted that the nonlinear term, q, is related to the square of m.

$$q = \alpha m^2 \tag{25}$$

We therefore define a calibration coefficient, α, which is theoretically a function only of the characteristics of the detector.

$$\alpha = \frac{a}{b^2} \tag{26}$$

The Top-Level Calibration Equation

Expressed in terms of these three calibration coefficients (m, L_o, and α), Eq. 24 becomes

$$V_s = \alpha m^2 \left(L_o + D_s \sum_{\lambda=\lambda_1}^{\lambda_n} \rho_{\lambda,s} \left(L_{\lambda,s} - B_{\lambda,mir} \right) R_{\lambda,opt} \Delta\lambda \right)^2 + m \left(L_o + D_s \sum_{\lambda=\lambda_1}^{\lambda_n} \rho_{\lambda,s} \left(L_{\lambda,s} - B_{\lambda,mir} \right) R_{\lambda,opt} \Delta\lambda \right) \tag{27}$$

Section 4

Determination of the Earth Scene Spectral Radiance

Applying Eq. 27 to the Earth scene yields

$$V_{ev} = \alpha m^2 \left(L_o + D_{ev} \sum_{\lambda=\lambda_1}^{\lambda_n} \rho_{\lambda,ev} \left(L_{\lambda,ev} - B_{\lambda,mir} \right) R_{\lambda,opt} \Delta\lambda \right)^2 + m \left(L_o + D_{ev} \sum_{\lambda=\lambda_1}^{\lambda_n} \rho_{\lambda,ev} \left(L_{\lambda,ev} - B_{\lambda,mir} \right) R_{\lambda,opt} \Delta\lambda \right) \quad (28)$$

Since the spectral signature for the Earth scene is not known, it will be assumed flat, and an average value of the Earth scene radiance will be factored out of the summation. This term is referred to as the spectral radiance of the Earth scene and is the Level 1B product of the calibration algorithm. Eq. 28 now becomes

$$\begin{aligned} V_{ev} = {} & \alpha m^2 \left(L_o + D_{ev} L_{ev} \sum_{\lambda=\lambda_1}^{\lambda_n} \rho_{\lambda,ev} R_{\lambda,opt} \Delta\lambda - D_{ev} \sum_{\lambda=\lambda_1}^{\lambda_n} \rho_{\lambda,ev} B_{\lambda,mir} R_{\lambda,opt} \Delta\lambda \right)^2 \\ & + m \left(L_o + D_{ev} L_{ev} \sum_{\lambda=\lambda_1}^{\lambda_n} \rho_{\lambda,ev} R_{\lambda,opt} \Delta\lambda - D_{ev} \sum_{\lambda=\lambda_1}^{\lambda_n} \rho_{\lambda,ev} B_{\lambda,mir} R_{\lambda,opt} \Delta\lambda \right) \end{aligned} \quad (29)$$

where the Level 1B product, L_{ev}, is defined just before incidence with the scan mirror as

$$L_{ev} = \frac{\sum_{\lambda=\lambda_1}^{\lambda_n} L_{\lambda,ev} R_{\lambda,tot} \Delta\lambda}{\sum_{\lambda=\lambda_1}^{\lambda_n} R_{\lambda,tot} \Delta\lambda} \quad (30)$$

Solving Eq. 29 for the Earth scene spectral radiance yields

$$L_{ev} = \frac{-1 + \sqrt{1 + 4\alpha V_{ev}} + 2\alpha m \left(-L_o + D_{ev} \sum_{\lambda=\lambda_1}^{\lambda_n} \rho_{ev} B_{\lambda,mir} R_{\lambda,opt} \Delta\lambda \right)}{2\alpha m D_{ev} \sum_{\lambda=\lambda_1}^{\lambda_n} \rho_{ev} R_{\lambda,opt} \Delta\lambda} \quad (31)$$

With only two on-orbit calibrators for the MODIS infrared bands, it is only possible to solve for two calibration "coefficients" on-orbit. From the three calibrator pre-launch thermal vacuum tests, it will be possible to determined these three calibration coefficients for a set of instrument conditions. Because variation in the non-linear coefficient (α) with instrument conditions will have less effect on the output product than variation of the

other two calibration coefficients, α will be determined from the thermal vacuum tests for several sets of instrument conditions and treated as a constant unique to each combination of instrument and detector temperatures for the life of the mission. This value of α will be interpolated to the on-orbit conditions.

To determine the two on-orbit calibration coefficients (m and L_o), apply Eq. 27 to the space view and OBC blackbody. This yields two equations with two unknowns. Solving for these unknowns we get

$$L_o = \frac{-1 + \sqrt{1 + 4\alpha V_{sv}}}{2\alpha m} + D_{sv} \sum_{\lambda=\lambda_1}^{\lambda_n} \rho_{sv} \left(B_{\lambda,mir} - L_{\lambda,sv} \right) R_{\lambda,opt} \Delta\lambda \tag{32}$$

$$m = \frac{\sqrt{1 + 4\alpha V_{bb}} - \sqrt{1 + 4\alpha V_{sv}}}{2\alpha \left(\sum_{\lambda=\lambda_1}^{\lambda_n} \rho_{bb} \left(L_{\lambda,bb} - B_{\lambda,mir} \right) R_{\lambda,opt} \Delta\lambda + D_{sv} \sum_{\lambda=\lambda_1}^{\lambda_n} \rho_{sv} \left(B_{\lambda,mir} - L_{\lambda,sv} \right) R_{\lambda,opt} \Delta\lambda \right)} \tag{33}$$

Section 5

Corrections for Scan Mirror Reflectivity Changes On-Orbit

On-orbit, it is possible to create a scenario where D_{ev} may be determined for all Earth view scan angles. To do this, MODIS must view space through the Earth view at a scan angle of -23.4 degrees which corresponds to the same angle of incidence, φ_{bb}, with the scan mirror as the OBC blackbody (see Fig. 7). Since the detector footprint for these two scan angles is effectively identical in size, shape, and location on the scan mirror, this creates a situation where m and L_o can be calibrated without scan mirror dependencies.

From Fig. 7, it is apparent that

$$\varphi_{ev@bb} = \varphi_{bb} \tag{34}$$

Applying Eq. 27 to the view of cold space through the Earth viewport at the scan mirror angle which is to be scan mirror corrected relative to the value at the OBC blackbody view angle, yields

$$V_{ev} = \alpha m^2 \left(L_o - D_{ev} \sum_{\lambda=\lambda_1}^{\lambda_n} \rho_{\lambda,ev} B_{\lambda,mir} R_{\lambda,opt} \Delta\lambda \right)^2 + m \left(L_o - D_{ev} \sum_{\lambda=\lambda_1}^{\lambda_n} \rho_{\lambda,ev} B_{\lambda,mir} R_{\lambda,opt} \Delta\lambda \right) \tag{36}$$

Solving for D_{ev}

$$D_{ev} = \frac{1 - \sqrt{1 + 4\alpha V_{ev}} + 2\alpha m L_o}{2\alpha m \sum_{\lambda=\lambda_1}^{\lambda_n} \rho_{ev} B_{\lambda,mir} R_{\lambda,opt} \Delta\lambda} \tag{37}$$

To determine the calibration coefficients, apply Eq. 27 to the blackbody (bb) and to the view of cold space through the Earth viewport at the blackbody equivalent scan mirror angle of incidence (ev@bb). This yields two equations with two unknowns. Solving for these unknowns we get

$$L_o = \frac{-1 + \sqrt{1 + 4\alpha V_{ev@bb}}}{2\alpha m} + \sum_{\lambda=\lambda_1}^{\lambda_n} \rho_{bb} B_{\lambda,mir} R_{\lambda,opt} \Delta\lambda \tag{38}$$

$$m = \frac{\sqrt{1+4\alpha V_{bb}} - \sqrt{1+4\alpha V_{ev@bb}}}{2\alpha \sum_{\lambda=\lambda_1}^{\lambda_n} \rho_{bb} L_{\lambda,bb} R_{\lambda,opt} \Delta\lambda} \tag{39}$$

Since the corresponding space view angle of incidence, φ_{sv}, occurs in the Earth view, D_{sv} is equal to D_{ev} at that angle. However, since the space view will also view cold space during the spacecraft roll, D_{sv} can be calculated directly from Equations 37 (replace "ev" with "sv").

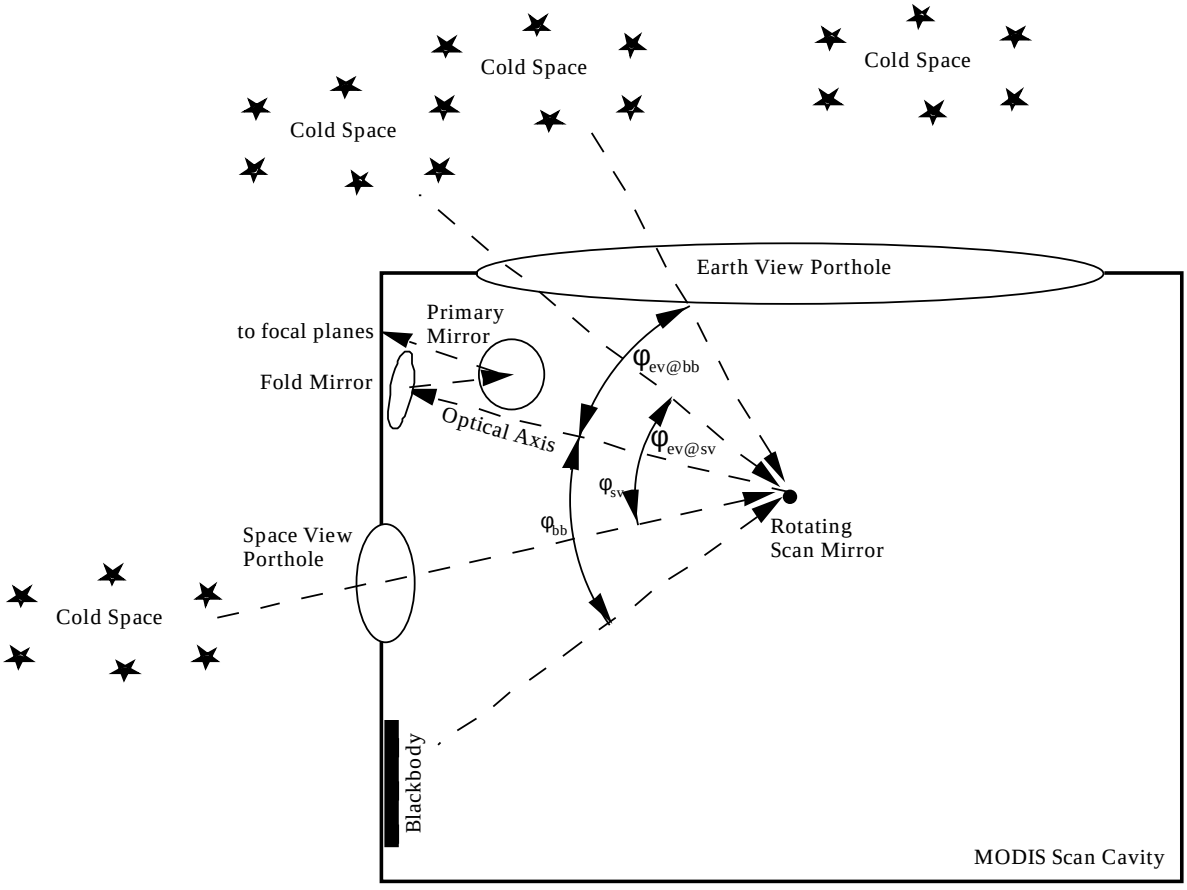

Figure 7. Scenario for deep space roll. Dashed line represents path of light ray to the detector. MODIS has an angle of incidence while viewing space through the Earth view porthole which is equivalent to the angle of incidence for each of the calibrators

Since detector flux variations with respect to scan angle while viewing space will be small it may be necessary to adjust the applied electronic gains to more adequately fill the A/D converter dynamic range and achieve better resolution. It is not in our current plan to

adjust these gains on-orbit, however the capability for adjustment is there and should be recognized.

Section 6

Determination of the Pre-Launch Non-Linear Coefficient

The thermal vacuum tests will use three calibration sources: the thermally isolated blackbody calibration source (bcs) the OBC blackbody (bb) and the space view source (svs). The nonlinear term can be determined for each scan and then averaged to obtain an effective value to take onto orbit. Applying the calibration equation (Eq. 27) to these three thermal vacuum calibrators results in three equations with three unknowns.

$$V_{bcs} = q\left(L_{og} + \Delta L_{bcs}\right)^2 + m\left(L_{og} + \Delta L_{bcs}\right) \tag{40}$$

$$V_{bb} = q\left(L_{og} + \Delta L_{bb}\right)^2 + m\left(L_{og} + \Delta L_{bb}\right) \tag{41}$$

$$\mathrm{V_{svs}} = \mathrm{q}\left(\mathrm{L_{og}} + \Delta \mathrm{L_{svs}}\right)^2 + \mathrm{m}\left(\mathrm{L_{og}} + \Delta \mathrm{L_{svs}}\right) \tag{42}$$

Where

$$\Delta L_{bcs} = \sum_{\lambda=\lambda_1}^{\lambda_n} \rho_{\lambda,bcs}\left(L_{\lambda,bcs} - B_{\lambda,mir}\right) R_{\lambda,opt} \Delta\lambda \tag{43}$$

$$\Delta L_{bb} = \sum_{\lambda=\lambda_1}^{\lambda_n} \rho_{\lambda,bb}\left(L_{\lambda,bb} - B_{\lambda,mir}\right) R_{\lambda,opt} \Delta\lambda \tag{44}$$

$$\Delta \mathrm{L_{svs}} = \sum_{\lambda=\lambda_1}^{\lambda_n} \rho_{\lambda,\mathrm{svs}}\left(\mathrm{L_{\lambda,svs}} - \mathrm{B_{\lambda,mir}}\right) \mathrm{R_{\lambda,opt}} \Delta\lambda \tag{45}$$

The variables m and q can then be obtained using determinants

$$m = \frac{A}{C} \tag{46}$$

$$q = \frac{B}{C} \tag{47}$$

Where

$$A = \begin{vmatrix} \left(\Delta L_{bcs} + L_{og}\right)^2 & \left(V_{bcs}\right) \\ \left(\Delta L_{bb} + L_{og}\right)^2 & \left(V_{bb}\right) \end{vmatrix} \tag{48}$$

$$B = \begin{vmatrix} \left(V_{bcs}\right) & \left(\Delta L_{bcs} + L_{og}\right) \\ \left(V_{bb}\right) & \left(\Delta L_{bb} + L_{og}\right) \end{vmatrix} \tag{49}$$

$$C = \begin{vmatrix} \left(L_{bcs} + L_{og}\right)^2 & \left(L_{bcs} + L_{og}\right) \\ \left(L_{bb} + L_{og}\right)^2 & \left(L_{bb} + L_{og}\right) \end{vmatrix} \tag{50}$$

Substitute Eq. 46 and Eq. 47 into Eq. 42

$$V_{svs} = \frac{B}{C}\left(\Delta L_{svs} + L_{og}\right)^2 + \frac{A}{C}\left(\Delta L_{svs} + L_{og}\right) \tag{51}$$

Eq. 51 can then be written as

$$B\left(\Delta L_{svs} + L_{og}\right)^2 + A\left(\Delta L_{svs} + L_{og}\right) - CV_{svs} = 0 \tag{52}$$

Solving for L_{og} yields

$$L_{og} = \frac{-y - \sqrt{y^2 - 4xz}}{2x} \tag{53}$$

Where

$$x = \left(\Delta L_{bb} - \Delta L_{bcs}\right)V_{svs} + \left(\Delta L_{bcs} - \Delta L_{svs}\right)V_{bb} + \left(\Delta L_{svs} - \Delta L_{bb}\right)V_{bcs} \tag{54}$$

$$y = \left(\Delta L_{bb}^2 - \Delta L_{bcs}^2\right)V_{svs} + \left(\Delta L_{bcs}^2 - \Delta L_{svs}^2\right)V_{bb} + \left(\Delta L_{svs}^2 - \Delta L_{bb}^2\right)V_{bcs} \tag{55}$$

$$z = \left(\Delta L_{bb}^2 \Delta L_{bcs} - \Delta L_{bcs}^2 \Delta L_{bb}\right)V_{svs} + \left(\Delta L_{bcs}^2 \Delta L_{svs} - \Delta L_{svs}^2 \Delta L_{bcs}\right)V_{bb} + \left(\Delta L_{svs}^2 \Delta L_{bb} - \Delta L_{bb}^2 \Delta L_{svs}\right)V_{bcs} \tag{56}$$

The negative root of the quadratic is most likely the appropriate root to use in Eq. 53. This is determined based on a consideration of what happens when the flux due to the optical background increases while the flux due to the scan mirror and image sources remain constant. For this scenario the pre-amplified voltages will increase for all three calibrators. Due to this, c may change more so than a and b. For this case, L_{og} must increase as z increases and the negative root must be used, except when $x<0$, $y>0$ and $z<0$.

However, since L_{og} is only determined pre-launch, it would be better and safer to determine the sign of the root by applying the thermal vacuum data to Eq. 53 for both signs of the root and using the root resulting in the greater value of L_{og}. Since L_{og} is defined as positive in the on-orbit algorithm this would insure the use of the correct root of Eq. 53.

From Equation 26 we see that

$$\alpha = \frac{q}{m^2} \tag{57}$$

Plugging Eq. 46 and Eq. 47 into Eq. 57 gives

$$\alpha = \frac{BC}{A^2} \tag{58}$$

Therefore the pre-launch calibration coefficient α is

$$\alpha = \frac{\left(V_{bcs}\left(\Delta L_{bb} + L_{og}\right) - V_{bb}\left(\Delta L_{bcs} + L_{og}\right)\right)\left(\left(\Delta L_{bb} + L_{og}\right)\left(\Delta L_{bcs} + L_{og}\right)^2 - \left(\Delta L_{bcs} + L_{og}\right)\left(\Delta L_{bb} + L_{og}\right)^2\right)}{\left(V_{bb}\left(\Delta L_{bcs} + L_{og}\right)^2 - V_{bcs}\left(\Delta L_{bb} + L_{og}\right)^2\right)^2} \tag{59}$$

The blackbody calibration source will be adjusted to several temperatures. Since it is thermally isolated from MODIS, these reference values may be used instead of the OBC blackbody to determine α. In this case, Eq. 59 might be rewritten replacing bcs with bcs1 and bb with bcs2. Eq. 59 could then be applied to each pair of blackbody calibration source temperature levels to determine an average value of α to be used on-orbit.

The current plan is to measure α at several patch and optics temperatures. This will enable us to apply the appropriate value by measuring the patch and optics temperatures on-orbit.

Section 7

Determination of the On-Board Blackbody Spectral Radiance

The spectral radiance from the OBC blackbody incident on the scan mirror can be determined every scan as

$$L_{\lambda,bb} = \varepsilon_{\lambda,bb} B_{\lambda,bb} + \frac{1-\varepsilon_{\lambda,bb}}{\pi}\left(\Omega_{cav} B_{\lambda,cav} + \Omega_{ev} B_{\lambda,Earth}\right) \quad (60)$$

where:

$$\Omega_{cav} + \Omega_{ev} = \pi \quad (61)$$

$\varepsilon_{\lambda,bb}$ = blackbody emissivity (measured pre-launch)
Ω_{cav} = effective solid angle of the scan cavity subtended at the blackbody
Ω_{ev} = effective solid angle of the Earth view porthole visible to the blackbody

Note the use of the notation ε_{bb} to denote the emissivity of the blackbody itself, and ρ_{bb} to denote the reflectivity of the scan mirror at the blackbody view angle. For the purposes of simple (but specific) notation in this document, ρ will refer to the reflectivity of the scan mirror with the subscript denoting the radiance source being viewed by the optics and ε will be refer to the emissivity of the Planck source viewed by the scan mirror

The twelve OBC blackbody thermistors will be averaged to obtained one effective temperature for the blackbody (see Section 2 for outlier rejection techniques). This is possible because the expected gradients will be small and the focal plane "footprint" covers about 90% of the blackbody for any single data sample. Fifteen OBC blackbody data frames will be available each scan for calibration.

The effective temperature of the scan cavity must be determined from appropriate thermistors within the scan cavity. This will be done by weighted averages of the pertinent scan cavity thermistor measurements (exact algorithm and thermistors are TBD). The effective temperature of the Earth is a fairly minor term in Eq. 3 (less than 1 part in a thousand). This radiance is the average temperature of the entire Earth scene (value is TBD) which directly illuminates the surface of the on-board blackbody.

The temperature of the OBC blackbody can be elevated to 315K and subsequently cooled down to ambient. This would present a possibility for the on-orbit determination of the nonlinear calibration term. However, due to the nonisothermal nature of this scenario, optical background drifts will occur and it will be a nontrivial "at best" effort to account for these drifts. The thermal calibration equation places no restriction on the OBC blackbody temperature and can be calibrated identically for both the normal and heated operational blackbody modes. However, a warning flag will be affixed to the data acquired during the heated mode.

The emissivity of the OBC blackbody might not be directly measured. If this is the case, measurements of the substrate material will be used to determine the OBC blackbody emissivity. The current opinion for determining the OBC blackbody emissivity in this manner is to assume that 10% of the radiance achieves only a single bounce, while the remaining radiance achieves four bounces within the v-groove surfaces. Current analyses shows that the on-board blackbody has a small but possibly significant residual polarization which may drop the desired blackbody emissivity below .992 for some MODIS bands.

The BCS will be used to test and further characterize the OBC blackbody (i.e. determining the OBC emissivity, etc.). This algorithm is TBD pending the methodology of these measurements. Ideally the temperature of the BCS would be adjusted to produce approximately the same signal as that of the OBC blackbody. This situation would bypass the requirement for knowledge of the detector non-linearities when calculating the OBC blackbody emissivity. Furthermore, the instrument temperature must be measured (ideally at several temperatures) to characterize the reflective components of the OBC blackbody.

Determination of the Planck Function Spectral Radiance

Since the desired units of spectral radiance is Watts per meter squared per micron per steradian, the Planck function is:

$$B_{\lambda,s} = \frac{2hc^2}{\pi\lambda^5\left(e^{(ch/\lambda kT_s)} - 1\right)} \qquad (62)$$

where:

h = Planck's constant $6.6256 \pm 0.0005 \times 10^{-34}$ W sec^2

c = Speed of light $2.997925 \pm .000003 \times 10^8$ m / sec

k = Boltzmann's constant $1.38054 \pm 0.00018 \times 10^{-23}$ W sec / K

Ts = temperature of the Planck source (i.e. scan mirror, blackbody, scan cavity, blackbody calibration source, etc.)

Section 8

Accounting for the Effects of DC Restore

The following are the current MCST algorithms for converting the MODIS digital number output of the analog to digital (A/D) converter into the pre-amplified voltages. These algorithms are essential to nonlinear corrections since a digital number by itself has no absolute meaning without its respective applied gains and offsets.

Determination of the Amplified Voltage Input to A/D Converter

The voltage across the A/D converter will be measured for each bin setting. A pre-launch lookup table will be used to convert the on-orbit digital output into the A/D voltage. This lookup table is represented here as $V_{A/D}\{DN - DN_o\}$. The telemetry will include the digital offset of the A/D converter as well as the digital number. If possible, this lookup table may be updated through ECAL measurement results.

Determination of the Pre-Amplified Voltage

To remove the applied electronic gains and offsets from the MODIS signal, it is necessary develop two algorithms: one for the photoconductive bands and one for the photovoltaic bands. The PV bands have four applied gain and one applied offset (see Fig. 8). The PC bands have two applied gains and two applied offsets (see Fig. 9). The offset for the PC bands is higher than for the PV bands since the detector flux due to the optical system is greater for higher wavelengths. Therefore, the PC circuit configuration must have two offsets to achieve an offset resolution comparable to that of the PV bands. The first PC offset is the course adjustment and the second PC offset is the fine adjustment.

To calibrate the photovoltaic bands, the pre-amplified voltage across the detector will be used, since it increases with detector flux. From the electronics circuit of Figure 8, we can see that

$$V_s^{PV} = \frac{V_{A/D}\{DN - DN_o\}}{G_1 G_2 G_3 G_4} - V_{DC1} \tag{64}$$

To calibrate the photoconductive bands, the pre-amplified voltage across the load resistor will be used, since it increases with detector flux. From the electronics circuit of Figure 9, we can see that

$$V_s^{PC} = \frac{V_{A/D}\{DN - DN_o\}}{G_1 G_2} - \frac{V_{DC2}}{G_1} - V_{DC1} \tag{65}$$

The superscript notation "PV" and "PC" is used here to more readily distinguish the appropriate equation for each detector circuit. It is important to note that the actual value for V_{DC1} and V_{DC2} will be negative.

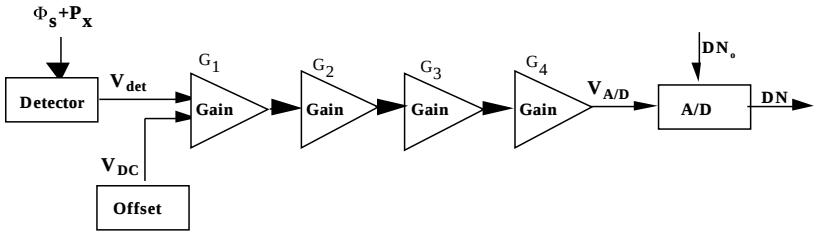

Figure 8. Electronics circuit design for the photovoltaic bands

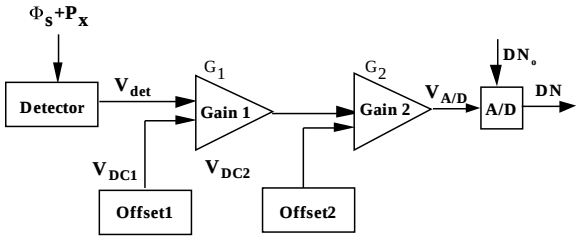

Figure 9. Electronics circuit design for the photoconductive bands

Section 9

Traceability of the OBC Blackbody to NIST

Thermal Traceability of the OBC Blackbody

The temperature of the OBC blackbody will be traced to NIST through the twelve thermistors embedded within its substrate. Each thermistor is directly traceable to NIST with an uncertainty of .005 K. Including factors such as 17 year drift, mechanical strain, interpolation, A/D digitization, and telemetry multiplexer, and uncertainty in the measurement of each thermistor becomes .028K. Including the effects due to thermistor potting and substrate gradients, the uncertainty of the OBC blackbody temperature becomes .062K. This meets the requirement of .1K as stated in the MODIS Specification.

Radiometric Traceability of the OBC Blackbody

The protoflight testing will be done with the BCS at several temperatures. Before the nonlinearity of the system can be determined, the OBC blackbody must be radiometrically calibrated to the BCS. This will enable the determination of the nonlinear term with three radiance levels each scan.

To radiometrically calibrate the OBC blackbody, the scans where the OBC blackbody and BCS have a similar temperature and digital output will provide the best results. For this case, the detector response can be assumed linear since the data points nearly overlap. In addition, the OBC blackbody must be elevated above the cavity temperature. This is necessary because the emissivity of the OBC blackbody is the key factor which must be calibrated to the BCS.

Calibration coefficients will be determined using the SVS and the BCS. These coefficients will then be applied to the digital output while viewing the OBC blackbody. From this, the emissivity of the OBC blackbody can be determined. The pertinent assumptions in this methodology is that the effective cavity temperature can be measured to 10K and the OBC blackbody temperature can be measured to .1K.

Section 10

Software Implementation: The Use of Look-Up Tables

This section translates the calibration equations into form which can be coded using lookup tables. Lookup table are necessary to reduce computer time required in summing spectrally across each detector channel.

Equations 31, 32, 33, and 60 can be arranged and combined whereby the number of lookup tables is minimized. This combination determines the apparent spectral radiance of the Earth scene as

$$L_{ev} = \frac{-1 + \sqrt{1 + 4\alpha V_{ev}}}{2\alpha m D_{ev} \sum_{\lambda=\lambda_1}^{\lambda_n} \rho_{ev} R \Delta\lambda} + \frac{-L_o + D_{ev} \sum_{\lambda=\lambda_1}^{\lambda_n} \rho_{ev} B_{mir} R \Delta\lambda}{D_{ev} \sum_{\lambda=\lambda_1}^{\lambda_n} \rho_{ev} R \Delta\lambda} \tag{71}$$

where

$$L_o = \frac{-1 + \sqrt{1 + 4\alpha V_{sv}}}{2\alpha m} + D_{sv} \left(\sum_{\lambda=\lambda_1}^{\lambda_n} \rho_{sv} B_{mir} R \Delta\lambda - \sum_{\lambda=\lambda_1}^{\lambda_n} \rho_{sv} B_{sv} R \Delta\lambda \right) \tag{72}$$

$$m = \frac{\sqrt{1 + 4\alpha V_{bb}} - \sqrt{1 + 4\alpha V_{sv}}}{2\alpha Z} \tag{73}$$

$$\begin{aligned} Z = & \sum_{\lambda=\lambda_1}^{\lambda_n} \rho_{bb} \varepsilon_{bb} B_{bb} R \Delta\lambda + \frac{\Omega_{cav}}{\pi} \left(\sum_{\lambda=\lambda_1}^{\lambda_n} \rho_{bb} B_{cav} R \Delta\lambda - \sum_{\lambda=\lambda_1}^{\lambda_n} \rho_{bb} \varepsilon_{bb} B_{cav} R \Delta\lambda \right) \\ & + \frac{\Omega_{ev}}{\pi} \left(\sum_{\lambda=\lambda_1}^{\lambda_n} \rho_{bb} B_{Earth} R \Delta\lambda - \sum_{\lambda=\lambda_1}^{\lambda_n} \rho_{bb} \varepsilon_{bb} B_{Earth} R \Delta\lambda \right) \\ & - \sum_{\lambda=\lambda_1}^{\lambda_n} \rho_{bb} B_{mir} R \Delta\lambda + D_{sv} \left(\sum_{\lambda=\lambda_1}^{\lambda_n} \rho_{sv} B_{mir} R \Delta\lambda - \sum_{\lambda=\lambda_1}^{\lambda_n} \rho_{sv} B_{sv} R \Delta\lambda \right) \end{aligned} \tag{74}$$

The aforementioned scientific notation translates into the following proposed lookup table notation as

$$\sum_{\lambda=\lambda_1}^{\lambda_n} \rho_s B_s R \Delta\lambda = Therm\_Planck(b)(T_s, \rho_s, d)$$

$$\sum_{\lambda=\lambda_1}^{\lambda_n} \rho_{bb} \varepsilon_{bb} B_T R \Delta\lambda = Therm\_BB(T_{bb}, d)$$

$$\sum_{\lambda=\lambda_1}^{\lambda_n} \rho_{sv} B_{sv} R \Delta\lambda = Therm\_Space(T_{sv}, d)$$

$$\sum_{\lambda=\lambda_1}^{\lambda_n} \rho_{ev} R \Delta\lambda = Therm\_Sum(d)$$

$$Vad_s = Therm\_Vad(ad\#, DN_s - DN_o)$$

$$\alpha = Therm\_Alpha(T_{inst}, T_{det}, d)$$

$$D_s = Therm\_Scan\_Angle(f, d)$$

The required sizes for each of these tables is TBD.

Expressed in table notational form, the apparent spectral radiance of the Earth scene is

$$L_{ev}(f,d) = \frac{-1 + \sqrt{1 + 4\ Therm\_Alpha(T_{inst}, T_{det}, d)\ V_{ev}(f,d)}}{2m(d)\ Therm\_Alpha(T_{inst}, T_{det}, d)\ Therm\_Scan\_Angle(f,d)\ \ Therm\_Sum(d)} + \frac{-L_o(d) + Therm\_Scan\_Angle(f,d)\ \ Therm\_Planck(b)(T_{mir}, \rho_{ev}, d)}{Therm\_Scan\_Angle(f,d)\ \ Therm\_Sum(d)} \tag{75}$$

where

$$L_o(d) = \frac{-1 + \sqrt{1 + 4V_{sv}(d)\ Therm\_Alpha(T_{inst}, T_{det}, d)}}{2m(d)\ Therm\_Alpha(T_{inst}, T_{det}, d)} + Therm\_Scan\_Angle(f,d)\left(Therm\_Planck(b)(T_{mir}, \rho_{sv}, d) - Therm\_Space(T_{sv}, d)\right) \tag{76}$$

$$m(d) = \frac{\sqrt{1 + 4Therm\_Alpha(T_{inst}, T_{det}, d)V_{bb}(d)} - \sqrt{1 + 4Therm\_Alpha(T_{inst}, T_{det}, d)V_{sv}(d)}}{2Therm\_Alpha(T_{inst}, T_{det}, d)Z(d)} \tag{77}$$

$$Z(d) = Therm\_BB(T_{bb}, d) + \frac{\Omega_{cav}}{\pi}\left(Therm\_Planck(b)(T_{cav}, \rho_{bb}, d) - Therm\_BB(T_{cav}, d)\right) \tag{78}$$

$$+ \frac{\Omega_{ev}}{\pi}\left(Therm\_Planck(b)(T_{Earth}, \rho_{bb}, d) - Therm\_BB(T_{Earth}, d)\right) - Therm\_Planck(b)(T_{mir}, \rho_{bb}, d) + Therm\_Scan\_Angle(f,d)\left(Therm\_Planck(b)(T_{mir}, \rho_{bb}, d) - Therm\_Space(T_{sv}, d)\right) \tag{79}$$

For bands 20-25, 27-30:

$$V_{ev}(d) = \frac{Vad(ad\#, DN_{ev}(f) - DN_o)}{G_1(d)G_2(d)G_3(d)G_4(d)} - V_{DC1}(d) \quad (80)$$

$$V_{sv}(d) = \frac{Vad(ad\#, DN_{sv} - DN_o)}{G_1(d)G_2(d)G_3(d)G_4(d)} - V_{DC1}(d) \quad (81)$$

$$V_{bb}(d) = \frac{Vad(ad\#, DN_{bb} - DN_o)}{G_1(d)G_2(d)G_3(d)G_4(d)} - V_{DC1}(d) \quad (82)$$

For bands 31-36:

$$V_{ev}(d) = \frac{Vad(ad\#, DN_{ev}(f) - DN_o)}{G_1(d)G_2(d)} - \frac{V_{DC2}(d)}{G_1(d)} - V_{DC1}(d) \quad (83)$$

$$V_{sv}(d) = \frac{Vad(ad\#, DN_{sv} - DN_o)}{G_1(d)G_2(d)} - \frac{V_{DC2}(d)}{G_1(d)} - V_{DC1}(d) \quad (84)$$

$$V_{bb}(d) = \frac{Vad(ad\#, DN_{bb} - DN_o)}{G_1(d)G_2(d)} - \frac{V_{DC2}(d)}{G_1(d)} - V_{DC1}(d) \quad (85)$$

Section 11

Uncertainty Analysis & Simulation Model

An analysis of the sensitivity of the Level 1B product to individual uncertainties in the on-orbit and pre-launch measured data was achieved through a simulated data model. This model assumes a quadratic relationship between detector incident radiant power and the resultant pre-amplified focal plane voltage. This quadratic relationship of the detector is identical for all bands. This nonlinearity is 10% for the dynamic range of band 31 (varies from band to band due to differing dynamic ranges and optical transmissions). This model assumed the apparent spectral radiance to be the Ltyp value defined in the MODIS specification.

The nominal values of the various thermistors inside the instrument were set to hopefully yield the most conclusive and realistic uncertainty results (i.e. OBC blackbody differs by 5K from the instrument to yield emissivity dependency).

For each nominal value, an uncertainty was added to the value and sent through the calibration equation to yield a Level 1B output product uncertainty for each independent data parameter. These uncertainty results were then root sum squared for all the data parameters to obtain a total uncertainty for each band.

The following charts show the simulated data set and a band by band breakdown of the perturbation parameters.

Band	Gain1	Gain2	Gain3	Gain4	Vdc1	Vdc2	Rad	DNbb	DNsv	DNev
20	12.61	15.00	15.00	15.00	-5.27E-06	0.00E+00	819.2	752	100	911
21	0.80	15.00	15.00	15.00	-2.66E-06	0.00E+00	819.2	121	100	191
22	32.03	15.00	15.00	15.00	-2.14E-06	0.00E+00	819.2	991	100	1195
23	26.70	15.00	15.00	15.00	-2.80E-06	0.00E+00	819.2	1017	100	1221
24	25.81	15.00	15.00	15.00	-7.76E-06	0.00E+00	819.2	1638	100	322
25	23.16	15.00	15.00	15.00	-8.17E-06	0.00E+00	819.2	1650	100	812
27	1.34	15.00	15.00	15.00	-3.18E-04	0.00E+00	819.2	2066	100	489
28	1.51	15.00	15.00	15.00	-2.98E-04	0.00E+00	819.2	2136	100	729
29	1.15	15.00	15.00	15.00	-4.28E-04	0.00E+00	819.2	1990	100	2167
30	1.27	15.00	15.00	15.00	-4.76E-04	0.00E+00	819.2	2367	100	1057
31	31.36	93.75	0.00	0.00	-5.45E-04	-5.70E-03	819.2	2207	100	2361
32	42.20	93.75	0.00	0.00	-6.61E-04	-9.30E-03	819.2	2259	100	2406
33	102.09	93.75	0.00	0.00	-3.82E-04	-1.30E-02	819.2	2539	100	1604
34	119.58	93.75	0.00	0.00	-3.84E-04	-1.53E-02	819.2	2550	100	1405
35	123.09	93.75	0.00	0.00	-3.76E-04	-1.54E-02	819.2	2561	100	1226
36	117.79	93.75	0.00	0.00	-3.35E-04	-1.31E-02	819.2	2572	100	901
31hi	15.52	93.75	0.00	0.00	-5.45E-04	-2.82E-03	819.2	1143	100	3172
32hi	21.55	93.75	0.00	0.00	-6.61E-04	-4.75E-03	819.2	1202	100	3172

Band 20 Uncertainty Analysis

Parameter	Nominal	Budget	Perturbation	Uncertainty (%Ltyp)
Temp Blackbody	295	0.1K	295.1	0.438
Temp Space	85	10K	85	0.000
Temp Cavity	290	10K	300	0.347
Temp Mirror	290	1K	291	0.007
Temp Earth Eff.	250	50K	300	0.024
Omega Earth	0.08159265	1%	0.08240858	0.000
Omega Cavity	3.06	1%	3.0906	0.006
Alpha	-39.236111		-104.055429	0.030
Gain1	12.6118818	1%	12.73800061	0.000
Gain2	15	1%	15.15	0.000
Gain3	15	1%	15.15	0.000
Gain4	15	1%	15.15	0.000
Vdc1	-5.272E-06	1%	-5.3247E-06	0.000
Vdc2	n/a	1%	n/a	0.000
DNbb	752.011774	1 bit + NEdL	754.7441067	0.419
DNsv	100			
DNev	910.874258			
Emiss_bb	0.99196458	0.004	0.995964579	0.088
Wavelength	3.75	0.10%	3.75375	0.803
Delta_sv/bb	1	0.10%	1.001	0.016
Delta_ev/bb	1	0.10%	1.001	0.036
Bandwidth	0.18	7	7.18	0.000
Rad	819.2	1%	827.392	0.000
Level 1B Radiance Uncertainty (Root Sum Squared)				1.069

Band 22 Uncertainty Analysis

Parameter	Nominal	Budget	Perturbation	Uncertainty (%Ltyp)
Temp Blackbody	295	0.1K	295.1	0.415
Temp Space	85	10K	85	0.000
Temp Cavity	290	10K	300	0.333
Temp Mirror	290	1K	291	0.004
Temp Earth Eff.	250	50K	300	0.024
Omega Earth	0.08159	1%	0.08240858	0.000
Omega Cavity	3.06	1%	3.0906	0.006
Alpha	-39.236		-173.873949	0.031
Gain1	32.0281	1%	32.34834693	0.000
Gain2	15	1%	15.15	0.000
Gain3	15	1%	15.15	0.000
Gain4	15	1%	15.15	0.000
Vdc1	-2E-06	1%	-2.1623E-06	0.000
Vdc2	n/a	1%	n/a	0.000
DNbb	991.149	1 bit + NEdL	995.251468	0.460
DNsv	100			
DNev	1195.32			
Emiss_bb	0.99186	0.004	0.995856916	0.084
Wavelength	3.959	0.10%	3.962959	0.734
Delta_sv/bb	1	0.10%	1.001	0.015
Delta_ev/bb	1	0.10%	1.001	0.034
Bandwidth	0.0594	7	7.0594	0.000
Rad	819.2	1%	827.392	0.000
Level 1B Radiance Uncertainty (Root Sum Squared)				1.021

Band 21 Uncertainty Analysis

Parameter	Nominal	Budget	Perturbation	Uncertainty (%Ltyp)
Temp Blackbody	295	0.1K	295.1	0.414
Temp Space	85	10K	85	0.000
Temp Cavity	290	1K	300	0.332
Temp Mirror	290	50K	291	0.014
Temp Earth Eff.	250	1%	300	0.024
Omega Earth	0.08159265	1%	0.08240858	0.000
Omega Cavity	3.06		3.0906	0.006
Alpha	-39.236111	1%	-183.301036	0.463
Gain1	0.80321158	1%	0.8112437	0.001
Gain2	15	1%	15.15	0.001
Gain3	15	1%	15.15	0.001
Gain4	15	1%	15.15	0.001
Vdc1	-2.657E-06	1%	-2.6838E-06	0.000
Vdc2	n/a	1 bit + NEdL	n/a	0.000
DNbb	120.892767			
DNsv	100			
DNev	190.740674	0.004	190.7406745	0.000
Emiss_bb	0.99185692	0.10%	0.995856916	0.084
Wavelength	3.959	0.10%	3.962959	0.734
Delta_sv/bb	1	0.10%	1.001	0.062
Delta_ev/bb	1	7	1.001	0.081
Bandwidth	0.0594	1%	7.0594	0.000
Rad	819.2	1	827.392	0.001
Level 1B Radiance Uncertainty (Root Sum Squared)				7.090

Band 23 Uncertainty Analysis

Parameter	Nominal	Budget	Perturbation	Uncertainty (%Ltyp)
Temp Blackbody	295	0.1K	295.1	0.406
Temp Space	85	10K	85	0.000
Temp Cavity	290	10K	300	0.327
Temp Mirror	290	1K	291	0.006
Temp Earth Eff.	250	50K	300	0.024
Omega Earth	0.08159265	1%	0.08240858	0.000
Omega Cavity	3.06	1%	3.0906	0.006
Alpha	-39.236111		-151.715764	0.032
Gain1	26.6982534	1%	26.96523597	0.000
Gain2	15	1%	15.15	0.000
Gain3	15	1%	15.15	0.000
Gain4	15	1%	15.15	0.000
Vdc1	-2.804E-06	1%	-2.8321E-06	0.000
Vdc2	n/a	1%	n/a	0.000
DNbb	1016.61191	1 bit + NEdL	1020.707831	0.447
DNsv	100			
DNev	1221.41443			
Emiss_bb	0.99181004	0.004	0.995810039	0.082
Wavelength	4.05	0.10%	4.05405	0.706
Delta_sv/bb	1	0.10%	1.001	0.015
Delta_ev/bb	1	0.10%	1.001	0.033
Bandwidth	0.0608	7	7.0608	0.000
Rad	819.2	1%	827.392	0.000
Level 1B Radiance Uncertainty (Root Sum Squared)				0.989

Band 24 Uncertainty Analysis

Parameter	Nominal	Budget	Perturbation	Uncertainty (%Ltyp)
Temp Blackbody	295	0.1K	295.1	0.379
Temp Space	85	10K	85	0.000
Temp Cavity	290	10K	300	0.313
Temp Mirror	290	1K	291	0.115
Temp Earth Eff.	250	50K	300	0.024
Omega Earth	0.08159265	1%	0.08240858	0.000
Omega Cavity	3.06	1%	3.0906	0.007
Alpha	-39.236111		-112.629235	0.141
Gain1	25.8080992	1%	26.0661802	0.001
Gain2	15	1%	15.15	0.001
Gain3	15	1%	15.15	0.001
Gain4	15	1%	15.15	0.001
Vdc1	-7.764E-06	1%	-7.8416E-06	0.000
Vdc2	n/a	1%	n/a	0.000
DNbb	1637.82991	1 bit + NEdL	1641.60445	0.254
DNsv	100			
DNev	322.33491			
Emiss_bb	0.99159626	0.004	0.995596259	0.078
Wavelength	4.465	0.10%	4.469465	0.593
Delta_sv/bb	1	0.10%	1.001	0.509
Delta_ev/bb	1	0.10%	1.001	0.491
Bandwidth	0.065	7	7.065	0.000
Rad	819.2	1%	827.392	0.001
Level 1B Radiance Uncertainty (Root Sum Squared)				1.095

Band 25 Uncertainty Analysis

Parameter	Nominal	Budget	Perturbation	Uncertainty (%Ltyp)
Temp Blackbody	295	0.1K	295.1	0.366
Temp Space	85	10K	85	0.000
Temp Cavity	290	10K	300	0.304
Temp Mirror	290	1K	291	0.020
Temp Earth Eff.	250	50K	300	0.023
Omega Earth	0.08159265	1%	0.08240858	0.000
Omega Cavity	3.06	1%	3.0906	0.007
Alpha	-39.236111		-105.420871	0.089
Gain1	23.1580359	1%	23.38961628	0.001
Gain2	15	1%	15.15	0.001
Gain3	15	1%	15.15	0.001
Gain4	15	1%	15.15	0.001
Vdc1	-8.173E-06	1%	-8.2545E-06	0.000
Vdc2	n/a	1%	n/a	0.000
DNbb	1649.66702	1 bit + NEdL	1658.115999	0.548
DNsv	100			
DNev	811.894155			
Emiss_bb	0.9915705	0.004	0.995570502	0.076
Wavelength	4.515	0.10%	4.519515	0.581
Delta_sv/bb	1	0.10%	1.001	0.099
Delta_ev/bb	1	0.10%	1.001	0.082
Bandwidth	0.067	7	7.067	0.000
Rad	819.2	1%	827.392	0.001
Level 1B Radiance Uncertainty (Root Sum Squared)				0.946

Band 27 Uncertainty Analysis

Parameter	Nominal	Budget	Perturbation	Uncertainty (%Ltyp)
Temp Blackbody	295	0.1K	295.1	0.252
Temp Space	85	10K	85	0.000
Temp Cavity	290	10K	300	0.126
Temp Mirror	290	1K	291	0.068
Temp Earth Eff.	250	50K	300	0.012
Omega Earth	0.08159265	1%	0.08240858	0.000
Omega Cavity	3.06	1%	3.0906	0.005
Alpha	-39.236111		-44.1200389	0.261
Gain1	1.33879257	1%	1.352180492	0.019
Gain2	15	1%	15.15	0.019
Gain3	15	1%	15.15	0.019
Gain4	15	1%	15.15	0.019
Vdc1	-0.0003176	1%	-0.00032082	0.001
Vdc2	n/a	1%	n/a	0.000
DNbb	2065.81163	1 bit + NEdL	2070.284351	0.240
DNsv	100			
DNev	488.58142			
Emiss_bb	0.99488367	0.004	0.998883675	0.055
Wavelength	6.715	0.10%	6.721715	0.226
Delta_sv/bb	1	0.10%	1.001	0.378
Delta_ev/bb	1	0.10%	1.001	0.366
Bandwidth	0.36	7	7.36	0.000
Rad	819.2	1%	827.392	0.019
Level 1B Radiance Uncertainty (Root Sum Squared)				0.737

Band 28 Uncertainty Analysis

Parameter	Nominal	Budget	Perturbation	Uncertainty (%Ltyp)
Temp Blackbody	295	0.1K	295.1	0.228
Temp Space	85	10K	85	0.000
Temp Cavity	290	10K	300	0.087
Temp Mirror	290	1K	291	0.027
Temp Earth Eff.	250	50K	300	0.008
Omega Earth	0.08159265	1%	0.08240858	0.000
Omega Cavity	3.06	1%	3.0906	0.003
Alpha	-39.236111		-44.5652716	0.220
Gain1	1.51370165	1%	1.528838665	0.015
Gain2	15	1%	15.15	0.015
Gain3	15	1%	15.15	0.015
Gain4	15	1%	15.15	0.015
Vdc1	-0.000298	1%	-0.00030096	0.001
Vdc2	n/a	1%	n/a	0.000
DNbb	2136.21459	1 bit + NEdL	2142.043377	0.296
DNsv	100			
DNev	728.926472			
Emiss_bb	0.99610634	0.004	1.000106339	0.050
Wavelength	7.325	0.10%	7.332325	0.166
Delta_sv/bb	1	0.10%	1.001	0.207
Delta_ev/bb	1	0.10%	1.001	0.196
Bandwidth	0.3	7	7.3	0.000
Rad	819.2	1%	827.392	0.015
Level 1B Radiance Uncertainty (Root Sum Squared)				0.555

Band 29 Uncertainty Analysis

Parameter	Nominal	Budget	Perturbation	Uncertainty (%Ltyp)
Temp Blackbody	295	0.1K	295.1	0.196
Temp Space	85	10K	85	0.000
Temp Cavity	290	10K	300	0.062
Temp Mirror	290	1K	291	0.024
Temp Earth Eff.	250	50K	300	0.006
Omega Earth	0.08159265	1%	0.08240858	0.000
Omega Cavity	3.06	1%	3.0906	0.003
Alpha	-39.236111		-44.2196381	0.039
Gain1	1.14742407	1%	1.15889831	0.003
Gain2	15	1%	15.15	0.003
Gain3	15	1%	15.15	0.003
Gain4	15	1%	15.15	0.003
Vdc1	-0.0004281	1%	-0.00043236	0.000
Vdc2	n/a	1%	n/a	0.000
DNbb	1989.73954	1 bit + NEdL	1992.69022	0.163
DNsv	100			
DNev	2167.44997			
Emiss_bb	0.99675531	0.004	1.000755307	0.044
Wavelength	8.55	0.10%	8.55855	0.072
Delta_sv/bb	1	0.10%	1.001	0.008
Delta_ev/bb	1	0.10%	1.001	0.018
Bandwidth	0.3	7	7.3	0.000
Rad	819.2	1%	827.392	0.003
Level 1B Radiance Uncertainty (Root Sum Squared)				0.280

Band 30 Uncertainty Analysis

Parameter	Nominal	Budget	Perturbation	Uncertainty (%Ltyp)
Temp Blackbody	295	0.1K	295.1	0.177
Temp Space	85	10K	85	0.001
Temp Cavity	290	10K	300	0.069
Temp Mirror	290	1K	291	0.073
Temp Earth Eff.	250	50K	300	0.007
Omega Earth	0.08159265	1%	0.08240858	0.001
Omega Cavity	3.06	1%	3.0906	0.003
Alpha	-39.236111		-44.1872253	0.261
Gain1	1.26702398	1%	1.27969422	0.018
Gain2	15	1%	15.15	0.018
Gain3	15	1%	15.15	0.018
Gain4	15	1%	15.15	0.018
Vdc1	-0.0004761	1%	-0.00048084	0.002
Vdc2	n/a	1%	n/a	0.001
DNbb	2366.59525	1 bit + NEdL	2373.023977	0.306
DNsv	100			
DNev	1056.67693			
Emiss_bb	0.99597453	0.004	0.999974531	0.040
Wavelength	9.73	0.10%	9.73973	0.003
Delta_sv/bb	1	0.10%	1.001	0.136
Delta_ev/bb	1	0.10%	1.001	0.126
Bandwidth	0.3	7	7.3	0.001
Rad	819.2	1%	827.392	0.018
Level 1B Radiance Uncertainty (Root Sum Squared)				0.491

Band 31 Uncertainty Analysis

Parameter	Nominal	Budget	Perturbation	Uncertainty (%Ltyp)
Temp Blackbody	295	0.1K	295.1	0.152
Temp Space	85	10K	85	0.000
Temp Cavity	290	10K	300	0.073
Temp Mirror	290	1K	291	0.010
Temp Earth Eff.	250	50K	300	0.008
Omega Earth	0.08159265	1%	0.08240858	0.000
Omega Cavity	3.06	1%	3.0906	0.005
Alpha	-39.236111		-43.5491683	0.048
Gain1	31.3583799	1%	31.67196373	0.004
Gain2	93.75	1%	94.6875	0.004
Vdc1	-0.0005449	1%	-0.00055036	0.000
Vdc2	-0.0056958	1%	-0.0057528	0.000
DNbb	2206.94599	1 bit + NEdL	2209.61192	0.133
DNsv	100			
DNev	2360.73545			
Emiss_bb	0.99508141	0.004	0.999081411	0.035
Wavelength	11.03	0.10%	11.04103	0.052
Delta_sv/bb	1	0.10%	1.001	0.007
Delta_ev/bb	1	0.10%	1.001	0.014
Bandwidth	0.5	7	7.5	0.000
Rad	819.2	1%	827.392	0.004
Level 1B Radiance Uncertainty (Root Sum Squared)				0.230

Band 32 Uncertainty Analysis

Parameter	Nominal	Budget	Perturbation	Uncertainty (%Ltyp)
Temp Blackbody	295	0.1K	295.1	0.140
Temp Space	85	10K	85	0.000
Temp Cavity	290	10K	300	0.085
Temp Mirror	290	1K	291	0.009
Temp Earth Eff.	250	50K	300	0.010
Omega Earth	0.08159265	1%	0.08240858	0.000
Omega Cavity	3.06	1%	3.0906	0.006
Alpha	-39.236111		-44.1169746	0.038
Gain1	42.2014063	1%	42.62342041	0.002
Gain2	93.75	1%	94.6875	0.002
Vdc1	-0.0006609	1%	-0.00066747	0.001
Vdc2	-0.0092964	1%	-0.00938935	0.000
DNbb	2259.20958	1 bit + NEdL	2261.77718	0.124
DNsv	100			
DNev	2405.87735			
Emiss_bb	0.99382897	0.004	0.99782897	0.033
Wavelength	12.02	0.10%	12.03202	0.087
Delta_sv/bb	1	0.10%	1.001	0.006
Delta_ev/bb	1	0.10%	1.001	0.013
Bandwidth	0.5	7	7.5	0.000
Rad	819.2	1%	827.392	0.002
Level 1B Radiance Uncertainty (Root Sum Squared)				0.230

Band 33 Uncertainty Analysis

Parameter	Nominal	Budget	Perturbation	Uncertainty (%Ltyp)
Temp Blackbody	295	0.1K	295.1	0.122
Temp Space	85	10K	85	0.008
Temp Cavity	290	10K	300	0.104
Temp Mirror	290	1K	291	0.046
Temp Earth Eff.	250	50K	300	0.005
Omega Earth	0.08159265	1%	0.08240858	0.007
Omega Cavity	3.06	1%	3.0906	0.001
Alpha	-39.236111		-49.4070021	0.171
Gain1	102.092097	1%	103.1130176	0.002
Gain2	93.75	1%	94.6875	0.002
Vdc1	-0.0003824	1%	-0.00038619	0.008
Vdc2	-0.0130123	1%	-0.01314239	0.008
DNbb	2539.27264	1 bit + NEdL	2546.244852	0.307
DNsv	100			
DNev	1603.93555			
Emiss_bb	0.99125553	0.004	0.995255531	0.023
Wavelength	13.335	0.10%	13.348335	0.132
Delta_sv/bb	1	0.10%	1.001	0.069
Delta_ev/bb	1	0.10%	1.001	0.047
Bandwidth	0.3	7	7.3	0.008
Rad	819.2	1%	827.392	0.002
Level 1B Radiance Uncertainty (Root Sum Squared)				0.421

Band 34 Uncertainty Analysis

Parameter	Nominal	Budget	Perturbation	Uncertainty (%Ltyp)
Temp Blackbody	295	0.1K	295.1	0.115
Temp Space	85	10K	85	0.013
Temp Cavity	290	10K	300	0.109
Temp Mirror	290	1K	291	0.063
Temp Earth Eff.	250	50K	300	0.001
Omega Earth	0.08159265	1%	0.08240858	0.013
Omega Cavity	3.06	1%	3.0906	0.004
Alpha	-39.236111		-51.2674755	0.216
Gain1	119.581381	1%	120.7771945	0.007
Gain2	93.75	1%	94.6875	0.007
Vdc1	-0.0003838	1%	-0.00038767	0.014
Vdc2	-0.0152997	1%	-0.01545267	0.013
DNbb	2550.3264	1 bit + NEdL	2556.757599	0.291
DNsv	100			
DNev	1404.78568			
Emiss_bb	0.99028836	0.004	0.994288355	0.017
Wavelength	13.635	0.10%	13.648635	0.145
Delta_sv/bb	1	0.10%	1.001	0.101
Delta_ev/bb	1	0.10%	1.001	0.068
Bandwidth	0.3	7	7.3	0.013
Rad	819.2	1%	827.392	0.007
Level 1B Radiance Uncertainty (Root Sum Squared)				0.446

Band 35 Uncertainty Analysis

Parameter	Nominal	Budget	Perturbation	Uncertainty (%Ltyp)
Temp Blackbody	295	0.1K	295.1	0.105
Temp Space	85	10K	85	0.022
Temp Cavity	290	10K	300	0.112
Temp Mirror	290	1K	291	0.084
Temp Earth Eff.	250	50K	300	0.006
Omega Earth	0.08159265	1%	0.08240858	0.021
Omega Cavity	3.06	1%	3.0906	0.011
Alpha	-39.236111		-51.8532422	0.264
Gain1	123.090871	1%	124.3217792	0.015
Gain2	93.75	1%	94.6875	0.015
Vdc1	-0.0003765	1%	-0.00038022	0.022
Vdc2	-0.0154461	1%	-0.01560055	0.022
DNbb	2561.18042	1 bit + NEdL	2567.101348	0.279
DNsv	100			
DNev	1226.08947			
Emiss_bb	0.98932118	0.004	0.99332118	0.008
Wavelength	13.935	0.10%	13.948935	0.161
Delta_sv/bb	1	0.10%	1.001	0.141
Delta_ev/bb	1	0.10%	1.001	0.091
Bandwidth	0.3	7	7.3	0.022
Rad	819.2	1%	827.392	0.015
Level 1B Radiance Uncertainty (Root Sum Squared)				0.487

Band 36 Uncertainty Analysis

Parameter	Nominal	Budget	Perturbation	Uncertainty (%Ltyp)
Temp Blackbody	295	0.1K	295.1	0.081
Temp Space	85	10K	85	0.047
Temp Cavity	290	10K	300	0.100
Temp Mirror	290	1K	291	0.142
Temp Earth Eff.	250	50K	300	0.030
Omega Earth	0.08159265	1%	0.08240858	0.047
Omega Cavity	3.06	1%	3.0906	0.035
Alpha	-39.236111		-51.7166127	0.360
Gain1	117.790301	1%	118.9682036	0.038
Gain2	93.75	1%	94.6875	0.038
Vdc1	-0.0003349	1%	-0.00033822	0.047
Vdc2	-0.013148	1%	-0.01327952	0.047
DNbb	2571.66285	1 bit + NEdL	2578.227004	0.338
DNsv	100			
DNev	901.14815			
Emiss_bb	0.988354	0.004	0.992354004	0.017
Wavelength	14.235	0.10%	14.249235	0.193
Delta_sv/bb	1	0.10%	1.001	0.263
Delta_ev/bb	1	0.10%	1.001	0.163
Bandwidth	0.3	7	7.3	0.047
Rad	819.2	1%	827.392	0.038
Level 1B Radiance Uncertainty (Root Sum Squared)				0.664

Band 31hi Uncertainty Analysis

Parameter	Nominal	Budget	Perturbation	Uncertainty (%Ltyp)
Temp Blackbody	295	0.1K	295.1	0.152
Temp Space	85	10K	85	0.001
Temp Cavity	290	10K	300	0.074
Temp Mirror	290	1K	291	0.002
Temp Earth Eff.	250	50K	300	0.009
Omega Earth	0.08159265	1%	0.08240858	0.001
Omega Cavity	3.06	1%	3.0906	0.006
Alpha	-39.236111		-43.5491683	1.798
Gain1	15.5236681	1%	15.67890473	0.136
Gain2	93.75	1%	94.6875	0.132
Vdc1	-0.0005449	1%	-0.00055036	0.014
Vdc2	-0.0028197	1%	-0.00284787	0.001
DNbb	1143.0236	1 bit + NEdL	1173.082293	2.933
DNsv	100			
DNev	3172			
Emiss_bb	0.99508141	0.004	0.999081411	0.036
Wavelength	11.03	0.10%	11.04103	0.051
Delta_sv/bb	1	0.10%	1.001	0.066
Delta_ev/bb	1	0.10%	1.001	0.070
Bandwidth	0.5	7	7.5	0.001
Rad	819.2	1%	827.392	0.132
Level 1B Radiance Uncertainty (Root Sum Squared)				3.454

Band 32hi Uncertainty Analysis

Parameter	Nominal	Budget	Perturbation	Uncertainty (%Ltyp)
Temp Blackbody	295	0.1K	295.1	0.142
Temp Space	85	10K	85	0.003
Temp Cavity	290	10K	300	0.087
Temp Mirror	290	1K	291	0.004
Temp Earth Eff.	250	50K	300	0.012
Omega Earth	0.08159265	1%	0.08240858	0.003
Omega Cavity	3.06	1%	3.0906	0.009
Alpha	-39.236111		-44.1169746	1.256
Gain1	21.5478179	1%	21.76329606	0.081
Gain2	93.75	1%	94.6875	0.078
Vdc1	-0.0006609	1%	-0.00066747	0.013
Vdc2	-0.0047467	1%	-0.00479415	0.003
DNbb	1202.48115	1 bit + NEdL	1229.63309	2.492
DNsv	100			
DNev	3172			
Emiss_bb	0.99382897	0.004	0.99782897	0.035
Wavelength	12.02	0.10%	12.03202	0.084
Delta_sv/bb	1	0.10%	1.001	0.065
Delta_ev/bb	1	0.10%	1.001	0.066
Bandwidth	0.5	7	7.5	0.003
Rad	819.2	1%	827.392	0.078
Level 1B Radiance Uncertainty (Root Sum Squared)				2.802

Nomenclature

V_s	focal plane voltage while viewing scene (s)
Φ_s	detector incident radiant flux attributed solely to the scan mirror and scene (s)
P_x	detector background flux and bias power (Joule heating)
a	second order detector gain term
b	first order detector gain term
$\tau_{\lambda,opt}$	spectral transmission of the static optic system
A_d	image area of the detector
ϕ_{port}	effective optical acceptance angle
$f_{eff}^{\#}$	effective focal ratio
$L_{\lambda,s}$	spectral radiance for scene (s)
$\rho_{\lambda,s}^{on-orbit}$	on-orbit spectral reflectivity of the scan mirror while viewing any scene (s)
$B_{\lambda,s}$	Planck function of the scan mirror temperature
$\tau_{\lambda,s}^{on-orbit}$	on-orbit spectral transmission of the static optics system
$k_{\lambda,opt}$	correction term for on-orbit change in static optics spectral transmission
$\tau_{\lambda,s}$	pre-launch spectral transmission of the static optics system
T_{opt}	total integrated transmittance of the static optics system
$R_{\lambda,opt}$	normalized spectral response of the static optics system
$R_{\lambda,tot}$	normalized spectral response of the total optical system
k_{opt}	correction term for on-orbit change in static optics effective transmission
$\delta_{\lambda,s}$	correction term for the on-orbit change in scan mirror spectral reflectivity
$\rho_{\lambda,s}$	pre-launch spectral reflectivity of the scan mirror while viewing any scene (s)
δ_s	correction term for the on-orbit change in scan mirror effective reflectivity
α	Pre-launch measured nonlinear calibration coefficient dependent on patch and optics temperature
L_o	calibration coefficient measured on-orbit which accounts for detector background flux and bias power (Joule heating)
q	second order term system gain calibration coefficient
m	first order term system gain calibration coefficient
D_s	correction term for on-orbit change the reflectivity of the scan mirror relative to the value at the OBC blackbody view angle
L_{ev}	Level 1B calibration product: apparent spectral radiance of the Earth view scene (Watts/µm/m^2/sr)
ϕ_s	angle between optical axis and scene (s) being scanned
ev@bb	refers to a view through the Earth view at the same angle of incidence with the mirror as a view of the nominal OBC blackbody
sv@bb	refers to a view through the Earth view at the same angle of incidence with the mirror as a view of the nominal space view

L_{og}	pre-launch calibration coefficient which accounts for detector background flux and bias power (Joule heating) during pre-launch conditions
$\varepsilon_{\lambda,bb}$	OBC blackbody emissivity
Ω_{cav}	effective solid angle of the scan cavity subtended at the OBC blackbody
Ω_{ev}	effective solid angle of the Earth view porthole subtended at the OBC blackbody
T_s	temperature of source (s)
$V_{A/D}\{\}$	Lookup table for voltage across the A/D converter
V_{DC1}	First stage voltage offset of the detector signal
V_{DC2}	Second stage voltage offset of the detector signal
G_1	First stage electronic gain of the detector signal
G_2	Second stage electronic gain of the detector signal
G_3	Third stage electronic gain of the detector signal
G_4	Fourth stage electronic gain of the detector signal
DN_o	Programmed digital offset of the A/D converter
s	scene (refers to any arbitrary radiance source)
bb	OBC blackbody
mir	scan mirror
sv	space view
ev	Earth scene viewed through Earth view porthole
bcs	blackbody calibration source (pre-launch calibrator)
svs	space view source (pre-launch calibrator)
cav	MODIS scan cavity

Bibliography

"MODIS infrared calibration algorithm derivation for ATBD 1995: draft", by Dan Knowles, August 7, 1995.

"Effects of low emissivity regions in using the on-board calibrator blackbody", by Dan Knowles and Ed Knight, March 2, 1995.

"OBC BB polarization", by Dan Knowles and Ed Knight, June 7, 1995.

"MODIS 1995 ATBD thermal calibration hybrid approach: traditional versus universal curve", by Dan Knowles, August 21, 1995.

"MODIS Level 1B input data set for the thermal bands", by Dan Knowles, September 19, 1995.

"Two-point calibration of non-linear PC HgCdTe channels", Infrared Phys. Technol. 36, by I. L. Goldberg, 1995.

"Gain Coefficients for radiometric calibration: version 2", PL3095-M03082, by Tom Pagano, October 4, 1993.

"MODIS updated transmission budgets", PL3095-Q02568, by Tom Kampe, May 13, 1993.

"Requirements for MODIS testing support software", 151868, by SBRC, November 18, 1994.

"Requirements for ambient calibration and testing (AC) support software", 151868, by SBRC 1994.

"Critical design review for the moderate resolution imaging spectroradiometer (MODIS)" vol. 2, by SBRC, 18-20 January, 1994.

"Critical design review for the moderate resolution imaging spectroradiometer (MODIS)" vol. 3, by SBRC, 18-20 January, 1994.

"Master curve approach applied to EM test data", PL3095-N05275, by Tom Pagano, September 7, 1995.

"Equations for the DC restore algorithm evaluated by data from the radiometric math model for the photo-voltaic bands 1-30", PL3095-M00832, by Tom Pagano, March 31, 1992.

"Equations for the DC restore algorithm evaluated by data from the radiometric math model for the photo-conductive bands 31-36", PL3095-M00890, by Tom Pagano, April 1, 1992.

"Operational in-flight calibration procedures (preliminary report)", CDRL 404, by SBRC, 1994.

"Gain/Offset and SNR algorithms for MODIS (preliminary)", PL3095-M02698, by Tom Pagano, June 29, 1993.

Section 9

Cutout
Traceability of the OBC Blackbody to NIST

Thermal Traceability of the OBC Blackbody

The temperature of the OBC blackbody will be traced to NIST through the twelve thermistors embedded within its substrate. Each thermistor is directly traceable to NIST with an uncertainty of .005 K. Including factors such as 17 year drift, mechanical strain, interpolation, A / D digitization, and telemetry multiplexer, and uncertainty in the measurement of each thermistor becomes .028K. Including the effects due to thermistor potting and substrate gradients, the uncertainty of the OBC blackbody temperature becomes .062K. This meets the requirement of .1K as stated in the MODIS Specification.

Radiometric Traceability of the OBC Blackbody

The protoflight testing will be done with the BCS at several temperatures. Before the nonlinearity of the system can be determined, the OBC blackbody must be radiometrically calibrated to the BCS. This will enable the determination of the nonlinear term with three radiance levels each scan.

To radiometrically calibrate the OBC blackbody, the scans where the OBC blackbody and BCS have a similar temperature and digital output will provide the best results. For this case, the detector response can be assumed linear since the data points nearly overlap. In addition, the OBC blackbody must be elevated above the cavity temperature. This is necessary because the emissivity of the OBC blackbody is the key factor which must be calibrated to the BCS.

Calibration coefficients will be determined using the SVS and the BCS. These coefficients will then be applied to the digital output while viewing the OBC blackbody. From this, the emissivity of the OBC blackbody can be determined. The pertinent assumptions in this methodolgy is that the effective cavity temperature can be measured to 10K and the OBC blackbody temperature can be measured to .1K.

For the moment, assuming a monochromatic radiance source for simplicity of notation, the radiance exitting the scan mirror (notated with the prime mark) while viewing the OBC blackbody can be determined from the digital counts as

$$L'_{bb} = L'_{svs} + \left(\frac{L'_{bcs} - L'_{svs}}{DN_{bcs} - DN_{svs}}\right)\left(DN_{bb} - DN_{svs}\right) \tag{66}$$

Applying the effects of the scan mirror, Eq. 66 can be expressed as

$$\sum_{\lambda=\lambda_1}^{\lambda_n} \rho_{bb} L_{bb} R_{opt} \Delta\lambda = X_1 \tag{67}$$

where

$$X_1 = \left(\frac{\sum_{\lambda=\lambda_1}^{\lambda_n} \rho_{bcs} L_{bcs} R_{opt} \Delta\lambda + \sum_{\lambda=\lambda_1}^{\lambda_n} \left(\rho_{svs} - \rho_{bcs} \right) B_{mir} R_{opt} \Delta\lambda}{DN_{bcs} - DN_{svs}} \right) \left(DN_{bb} - DN_{svs} \right) + \sum_{\lambda=\lambda_1}^{\lambda_n} \left(\rho_{bb} - \rho_{svs} \right) B_{mir} R_{opt} \Delta\lambda$$

Applying Eq. 60 to Eq. 67 yields

$$\sum_{\lambda=\lambda_1}^{\lambda_n} \rho_{bb} \left(\varepsilon_{bb} B_{bb} + \frac{1-\varepsilon_{bb}}{\pi} \left(\Omega_{cav} B_{cav} + \Omega_{ev} B_{chamber} \right) \right) R_{opt} \Delta\lambda = X_1 \tag{68}$$

Factoring out the OBC blackbody emissivity from the summation in Eq. 68 yields

$$\varepsilon_{bb} X_2 + X_3 = X_1 \tag{69}$$

where

$$X_2 = \frac{1}{\pi} \sum_{\lambda=\lambda_1}^{\lambda_n} \rho_{bb} \left(\pi B_{bb} - 1 \right) \left(\Omega_{cav} B_{cav} + \Omega_{ev} B_{chamber} \right) R_{opt} \Delta\lambda$$

$$X_3 = \frac{1}{\pi} \sum_{\lambda=\lambda_1}^{\lambda_n} \rho_{bb} \left(\Omega_{cav} B_{cav} + \Omega_{ev} B_{chamber} \right) R_{opt} \Delta\lambda$$

Solving Eq. 69 for the OBC blackbody emissivity yields

$$\varepsilon_{bb} = \frac{X_1 - X_3}{X_2} \tag{70}$$